Novel Electrospun Anatase/Poly(3,4-Ethylenedioxythiophene) Polystyrene Sulfonate-based Li-ion Battery Anodes and their Electrochemical Performances

by
VAHID CHARKHESHT

Submitted to the Graduate School of Engineering and Natural Sciences
in partial fulfillment of the requirements for the degree of
Master of Science

Sabancı University
December 2020

TITLE OF THE THESIS/DISSERTATION

APPROVED BY:

DATE OF APPROVAL: day/month/year

Novel Electrospun Anatase/Poly(3,4-Ethylenedioxythiophene) Polystyrene Sulfonate-based Li-ion Battery Anodes and their Electrochemical Performances

Vahid Charkhesht

Material Engineering and Science, MSc. Thesis, 2020

Thesis Supervisor: Prof. Dr. Selmiye Alkan Gürsel

Thesis Coadvisor: Dr. Begum Yarar Kaplan

ABSTARCT

Among the common batteries, LIBs as one of the pioneers in rechargeable batteries has become an intrinsic part of almost all the electronic devises. However, there are lots of rooms for improvement in terms of safety, working life, and charging pace. Using fibrous electrodes can improve the electrochemical behavior thanks to the enhancement of connection of the electrolyte with active material by increasing voids to facilitate the Li^+ transference. Electrospining as a simple, scalable, and cost-effective technique can build up the fibrous electrodes used in LIBs.

In this study, for the first time, highly conductive poly(3,4-ethylenedioxythiophene) polystyrene sulfonate (PEDOT:PSS) polymer was used as a carrier of electrospun TiO_2/CB-based anode. Due to the low viscosity of PEDOT:PSS solution, another carrier polymer with high molecular weight, PEO, was added to electrospinning ink to increase the viscosity and make the electrospinning process practical. A systematic and laborious optimizing work was performed to achieve the homogeneous ink composition and finally fibers with homogeneous particle distribution. The parameters include sonication type and time, PEO/PEDOT:PSS ratio, ink solid ratio, dispersants ratio (DMF/Water), PEO polymer ratio, and PEO molecular weight besides the operational parameters like operational voltage, needle to collector distant, polymer feeding rate and relative humidity. TGA, XRD, RAMAN, FTIR, and FE-SEM techniques were used to characterize the electrodes.

After electrode fabrication, electrochemical tests including galvanostatic charge/discharge, cyclic voltammetry, and electrochemical impedance spectroscopy were performed. Presence of PEDOT:PSS assists the anode performance by: i) improving the

conductivity and ii) increasing capacity due to the electrochemical activity of the polymer. Not only the achieved areal capacity (1.67 $mAh.cm^{-2}$) was comparable to the other studies, but also the gravimetric capacity (300 $mAh.g^{-1}$) was much higher than similar studies. These results are very promising for the next generation electrospun LIB electrodes fabricated using PEDOT: PSS as a binder/carrier.

Keywords: Li-ion battery, Electrospinning, PEDOT:PSS, Anode, Anatase

Yeni Elektrospun Anataz / Poli (3,4-Etilendioksitiyofen) Polistiren Sülfonat bazlı Li-ion Pil Anotları ve Elektrokimyasal Performansları

Vahid Charkhesht

MAT, M.Sc. Tezi, 2020

Tez danışmanı: Prof. Dr. Selmiye Alkan Gürsel

Tez eş danışmanı: Dr. Begum Yarar Kaplan

ÖZET

Bununla birlikte, Li-iyon pillerin (LIB) güvenlik, çalışma ömrü ve şarj hızı iyileştirilmesi gereken çok sayıda konuvardır. Lifli elektrotların kullanılması, Li^+ aktarımını kolaylaştırmak için lif içi ve lifler arası boşlukları artırarak elektrolitin aktif malzeme ile bağlantısının artırılması ile, pilin elektrokimyasal davranışı görülebilmektedir. Basit, ölçeklenebilir ve uygun maliyetli bir teknik olarak elektrodokuma, LIB'lerde kullanılan lifli elektrotların üretiminde kullanılabilir.

Bu çalışmada, elektrodokunmuş TiO_2/CB esaslı anotlar, yüksek iletkenliğe sahip bir polimer olanpoli(3,4-etilendioksitiyofen) polistiren sülfonat (PEDOT: PSS) polimeri literatürde ilk defa Li-iyon batarya anodu üretiminde taşıyıcı polimer olarak kullanılarak hazırlanmıştır. PEDOT:PSS çözeltileri düşük viskoziteye sahip olması nedeni ile, viskoziteyi artırmak ve elektrodokuma çözeltisine yüksek moleküler ağırlıklı başka bir taşıyıcı polimer olan poli (etilen oksit) (PEO) eklenmiştir. Homojen elektrodokuma çözeltisi bileşimini ve son olarak homojen parçacık dağılımına sahip lifleri elde etmek için sistematik ve düzenli bir optimizasyon çalışması gerçekleştirilmiştir. Sonikasyon tipi ve süresi, PEO / PEDOT: PSS oranı, elektrodokuma çözeltisindeki toplan katı oranı, çözücülerin oranı (DMF/Su), farklı moleküler ağırlığında PEO kullanılması gibi elektrodokuma çözeltisi parametrelerine ek olarak, uygulanan voltaj, iğne-kolektör uzaklığı, polimer besleme hızı, oran ve bağıl nem gibi sistem parametreleri de optimize edilmiş ve incelenmiştir.Elektrodokunmuş elektrotların karakterizasyonunda TGA, XRD, RAMAN, FTIR ve FE-SEM teknikleri kullanılmıştır.

Elektrot üretiminden sonra, galvanostatik şarj / deşarj, döngüsel voltametri ve elektrokimyasal empedans spektroskopisi olmak üzere birçok elektrokimyasal testyapılmıştır. Elde edilen sonuçlara göre PEDOT:PSS polimeri kullanılarak elde edilen elektrodokunmuş

anot şu sebeplerden dolayı yüksek performans göstermiştir: performansının i) daha yüksek elektrot iletkenliği ve ii) polimerin yüksek elektrokimyasal aktivitesinden dolayı kapasitenin artması. Batarya testleri sonucunda, bu tez ile üretilen elektrodokunmuş anodun alan kapasitesinin (1.67 $mAh.cm^{-2}$) diğer çalışmalarla karşılaştırılabilirolduğuve gravimetrik kapasitesinin (300 $mAh.g^{-1}$) benzer çalışmalardan çok daha yüksek seviyede olduğu gözlenmiştir. Elde edilen bu sonuçlar, PEDOT:PSS polimerinin bağlayıcı/taşıyıcı olarak kullanıldığı elektrodokunmuş elektrotların, gelecek nesil LIB için umut vericidir.

Anahtar Kelimeler: Li-iyon pil, Elektrodokuma, PEDOT:PSS, Anot, Anataz

AKNOWLEDGMENTS

First, I am really grateful to have chance to work under supervision of my thesis advisor, Prof. Selmiye Alkan Gürsel. Owning to possessing an integrous personality, I have always considered her as a family member rather than an academic collaborator. Without exaggeration, our world needs this type of people more than ever, and I have been so lucky to take full advantage of her emotional and motivational support.

I am also thankful to my fully respected co-advisor, Dr. Begum Yarar Kaplan, a symptom of perseverance and delegation. Thanks to her guiding and invaluable comments, I could improve my productivity to the highest possible extent.

I need to thank Dr. Alp Yurum owning to transferring of his knowledge and deepening my eyesight in my thesis. Without his novel solutions and thorough knowledge, there was no way I can complete this project.

I would like to thank my fellow friends Adnan Tas Demir, Naeimeh Rajabalizadeh, Bilal Iskandarani, Navid Haghmoradi, Buse Akbulut Kopuklu, Ahmet Can, Hamed Salimkhani, and Golnaz Naseri for their priceless help, whom I had the chance to know and collaborate with during the last two years of my academic life. They helped me to overcome all the difficulties and burdens on my way in completing this thesis.

Special thanks to my friends Mohammad Jafarpour, Ali Toufani, Ali Ansari Hamedani, Kamal Asadipakdel, Amin Abdollahzadeh, Shayan Ramazanzadeh, Roozbeh Saghatchi, and Hadi Abbaszadeh, who have supported me along the way during my study at Sabanci University.

The last but not the least, I would like to express my everlasting grace to my best friend and my wife, Mina Jafari, and my parents for supporting and encouraging me throughout my years of study and my life in general. This accomplishment would not have been possible without them.

Table of Contents

Table of Figures

Table of Tables

Table of Schemes

Chapter 1. Introduction

1.1 Importance of LIBs

The draining process of confined fossil-fuel resources and the related combustion side effects like environmental pollutions as well as global warming motivate researchers to develop green energy and storage technologies. Among them, the electric energy storage systems allow us to reuse the renewable natural energy resources [1].

Given electrochemical energy storage systems, lithium-ion secondary batteries (LIBs) possessing properties such as high energy density, long lifetime, and lightness have become an intrinsic part of human being life comprising a wide range of applications from electronic devices to the automotive industries since the last decade [2] [3]. Figure 1-1 illustrates a sample of the broad applications in today's life.

Figure 1-2 shows the ever-increasing need for LIBs will expand markets in the foreseeable future [2]. However, in order to achieve to an energy-sustainable economy, further improvement in energy densities, charge rate, cost, and safety is still imperatively demanded [4] [3] [5].

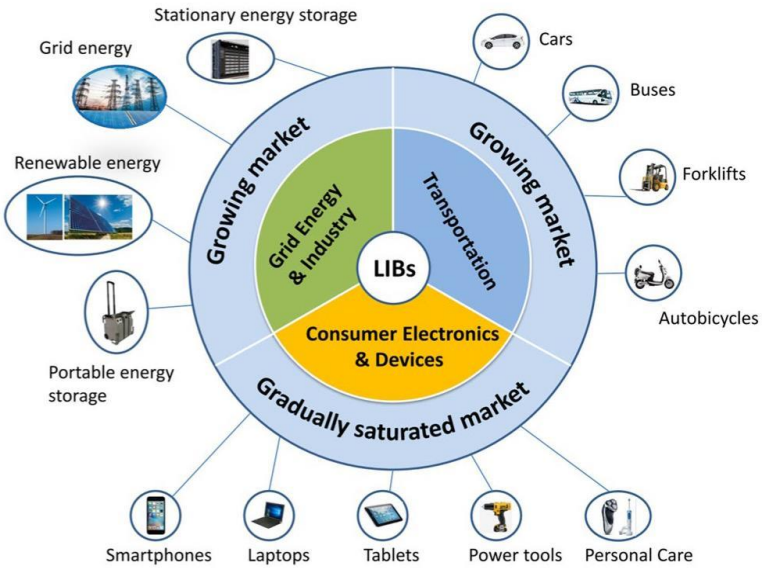

Figure 1-1. Applications for LiBs [1].

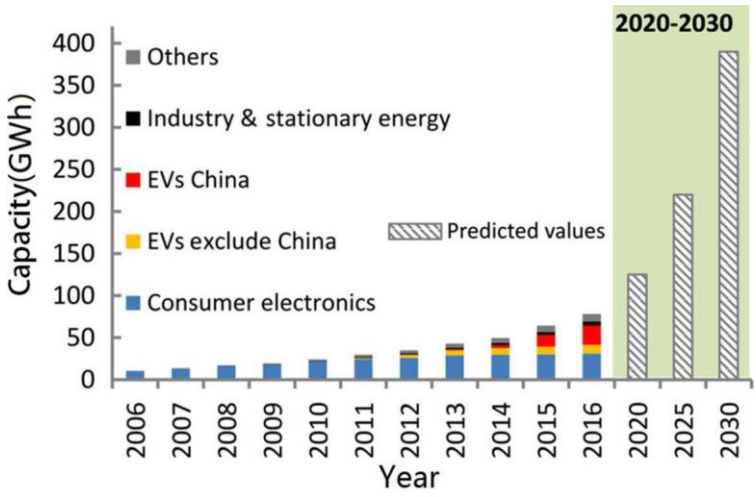

Figure 1-2. Present and future LIB market [1].

1.2 LIBs

After the primary discovery of LIBs during 1970s, it took about 20 years (near 1990) to achieve the 2nd generation of the LIBs which were rechargeable [6, 7]. LIBs are used as two electrode electrochemical systems. The major parts of this system are included of anode electrode, cathode electrode, separator, and electrolyte.

Li^+ diffusion in the layered structures along a two-dimensional (2D) interstitial space is deemed as the main mechanism for charging and discharging (Figure 1-3) [8]. Due to the low ionization energy of the Li, by opening the circuit, the electrons move through the resister and build up the needed current. On the other side, the Li^+ tends to insert within the cathode (materials with relatively higher ionization energy) assisted by the electrolyte. The process is called delithiation or discharge of the anode [9].

In return, when the anode of the battery is depleted with Li^+, by building up a sufficient potential between two electrodes, electrons and inserted Li^+ move through the reverse pathway to charge up the battery for another cycle usage. This process is called lithiation or charging of the anode [9]. The cycling process usually keeps on up to a few hundred cycles since there are loss of material (both cathode and anode) during repetitive insertion/extraction of Li^+ within the battery resulted in cracks on the electrodes and there will be a capacity loss.

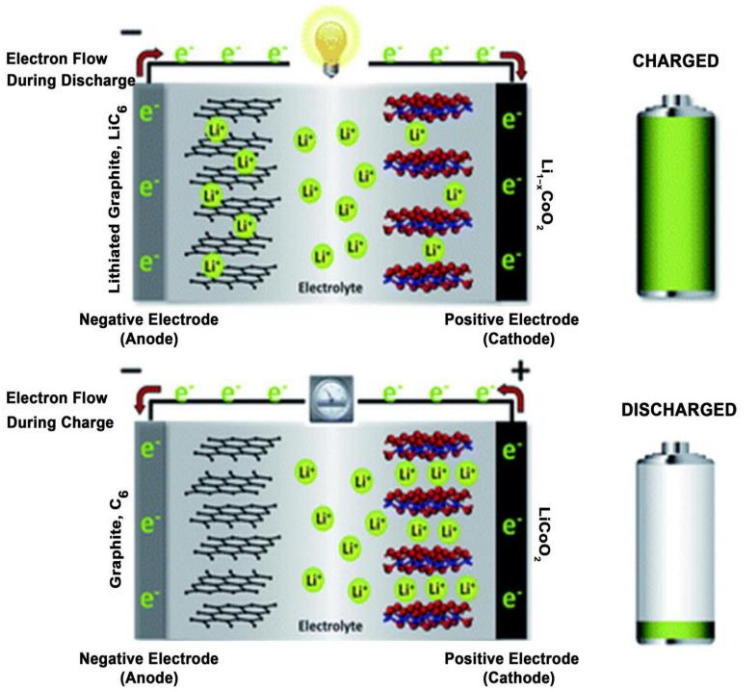

Figure 1-3. The charge/ discharge mechanism in the LIB batteries [9].

Dream to reach high energy density batteries which are economical and rechargeable becomes a reality when the graphite was chosen as the anode material instead of Li metal and a lithiated transition metal oxide, $LiMO_2$, was used as the source of lithium (the cathode electrode) [7]. One of the leading batteries was Graphite–LiCoO2, which was mostly used in the portable electronic devises: cameras, laptops, and cellular phones (Figure 1-3).

The main discharge reaction which occurs within the cathode is

$$Li^+ + e^- + 2Li_{0.5}CoO_2 \rightarrow 2LiCoO_2 \quad (1\text{-}1)$$

In which Li^+ was reduced in the cathode electrode. Due to the limited Li^+ extraction voltage (4.2 V vs. Li^+/Li) in the ionization process of the above reaction, only half of the theoretical capacity can be achieved (140 mAh.g^{-1}) [7]. Always the first process (charging) is in line with the oxidation or delithiation of the cathode. Similarly, the discharging process is accompanied with the delithiation and oxidation of the anode which is Graphite:

$$LiC_6 \rightarrow C_6 + Li^+ + e^- \quad (1\text{-}2)$$

Electrolyte within the LIBs plays a significant role to transfer the Li^+ within the two electrodes avoiding electrons passage and consequent short circuit. Alkyl carbonates were discovered as one of the promising electrolytes due to low weight, high conductivity, high dielectric constant, and high solubility of the Li salt [10]. The combination of ethylene carbonate (EC), dimethyl carbonate (DMC), and $LiPF_6$ resulted in the best among the commonly used electrolytes [7] because of high conductivity, relative high stability thanks to obtaining lower C-H bonds, formation of highly conductive solid electrolyte interface (SEI) layer for Li^+ bridging and protecting anode layer from detrimental superficial reactions [11].

Generally, gradual failure of the LIBs happens by recession of the voltage profile caused by the specific energy density decline over the course of operation (specific energy density = specific capacity × average operating voltage) [12]. Therefore, the major concern in LIB study field is providing higher energy densities. The most promising solution to overcome this challenge is replacing the traditional anodes and cathodes by high-capacity and high-voltage ones, respectively [13].

1.3 Anode

Carbonaceous anodes (graphite, carbon) are used as conventional anodes in commercial lithium-ion batteries thanks to their decent cyclability, abundance, and cost. However, inferior rate performance and safety issues caused by low Li^+ diffusion coefficient and lithium deposition, respectively, confine their broad utilization [14].

Owning to low lithium intercalation potential (0.1 V vs Li/Li^+), the safety problems can be intensified on fast changing rate thereby increasing the danger of short circuit ending up with thermal explosion [15]. Figure 1-4 shows different scenarios regarding low potential of the anodes like graphite: Intercalation of solvent molecules and exfoliation of the graphite layers, reduction of the electrolyte and producing the film on the surface, thickening of the SEI film, dissolution of the film by HF and dissolving the released cations of the transition metals, Li metal deposition [7]. As a result, the safer anode material is needed instead of graphite.

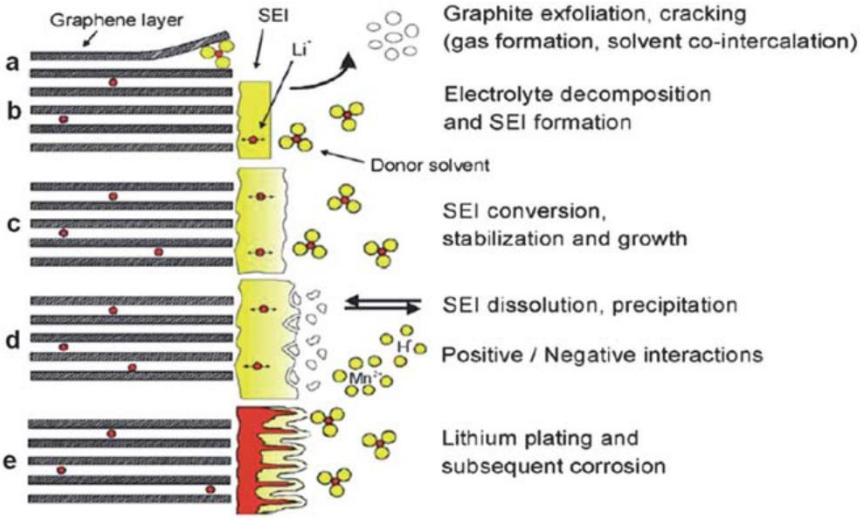

Figure 1-4. Different scenarios considering using graphite anode electrodes [7].

1.3.1 TiO_2 as an Anode Electrode

As one of the well-studied semiconducting metal oxides, the anatase-phase titanium (IV) oxide (TiO_2), grasp lots of interest in the varieties of applications in sensors, solar cells, photocatalysis, lithium ion batteries, etc. [16] [17].

Due to the high redox potential, decent capacity retention, high structural stability, low volume change (less than 4%), and long life cycles, anatase has been considered as one of the most promising anodes in LIBs [6]. Thereby obtaining a tetragonal unit cell, anatase can easily accommodate one lithium for every TiO_2 resulting in a theoretical theory of 335 $mAhg^{-1}$ [6]. Hence, it can be more efficient than the graphite anode material which consumes 6 carbon atoms to absorb one Li atom.

Utilizing anatase as an anode can impede the formation of lithium dendrites (lithium electroplating) because of its high discharge potential (1.7 V vs. Li/Li^+). Additionally, due to low volume expansion during lithiation and delithiation, the durability of cycles can be improved and formation of solid electrode interface can be inhibited as well [15]. These aspects of the TiO_2 improve the safety up to a comparative superior degree [14].

The following reaction shows the lithiation process of the anatase within the cell [18]:

$$TiO_2 + x\,Li^+ + xe^- \rightarrow Li_xTiO_2 \quad (1\text{-}3)$$

In which x values can be given by a number between 0.5 to 1.

The main challenge of the researchers is to increase the x values to a number close to 1. However, low electrical conductivity and Li^+ diffusivity inducing a poor rate capability are deemed as the major weak points of this material in LIB applications [6] [15], particularly in applications required high power density [14].

To overcome these drawbacks, many research have been conducted to enhance the insertion/extraction of Li^+ during the dis-/charge by generating facile open channels on the material [16]. Table 1-1 shows the research done on the TiO_2-based anode aiming to improve the specific capacity and cycling performances.

Thereby increasing the surface area, shorter Li^+ pass way can lead to the higher electrochemical kinetics in LIBs. Therefore, using TiO_2 nanoparticles (NP) could be efficient enough to reach maximize the specific capacity within the operation. However, the agglomeration and dissolution of the NPs impedes the proper productivity [14].

Hence, making porous TiO_2 [19], producing Micro-cone (MC) [20] and nanowire structures (NW) [21, 22] or building up a one-dimensional (1D) structures such as TiO_2 nanotubes (NT) [18, 23], nanorods (NR) [6, 16, 24, 25] can be more promising solution to problems confronted in NPs (some example of mentioned structures is shown in Figure 1-5). Even though, the extended surface area may result in the intensified side-reactions with the electrolyte compared to the bulk TiO_2 [16].

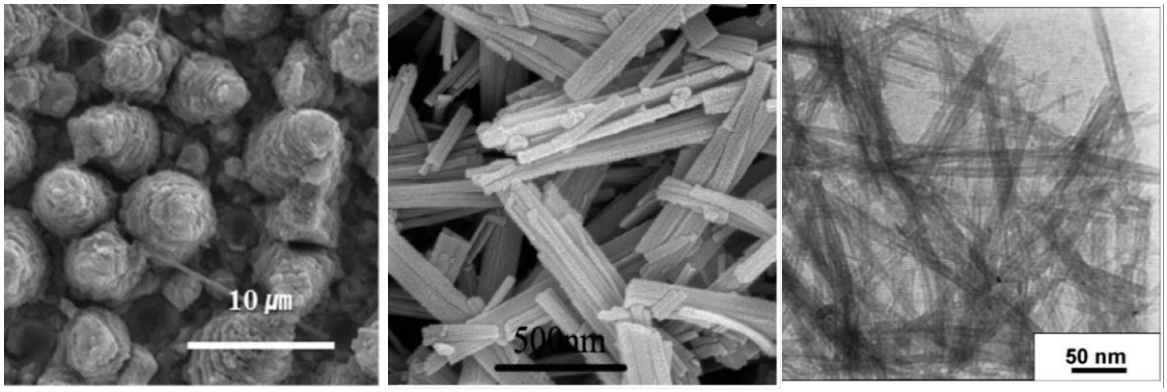

Figure 1-5. Micrographs of various modified TiO_2 structures: (a) MC [20], (b) NW [21], and NT [23].

Some research have targeted the conductivity deficiency of the anatase either by adding carbon nanotubes (CNT) [26] and reduced graphene oxides [15, 27, 28] or coating carbon [29] on the particles. Although the research done have improved the rate capability notably, there is still challenges to improve the specific capacity [6].

Table 1-1. Research done on the TiO_2 anode applied as a li-ion battery [15, 19].

Materials	Voltage [V vs Li/Li^+]	Current density [mA g^{-1}]	Specific capacity [mAh g^{-1}]	Cycling performances
TiO_2 fiber-graphene/carbon composites:				
TiO_2-graphene nanofibers	1.0–3.0	150	131	300
Reduced graphene oxide-supported TiO_2 fiber bundles	0.1–3.0	200	235	1000
		1000	150	
High performance N-doped mesoporous carbon decorated TiO_2 nanofibers	1.0–3.0	33	264	100
Mesoporous TiO_2 micro-fibers@nitrogen doped carbon composites	1.0–3.0	850	150	100
$OMTiO_2$–rGO-NF	1.0–3.0	33.5	295	–
		335	212	500
		838	168	–
TiO_2-graphene/carbon composites:				
Sandwich like graphene–TiO_2 nanosheets	1.0–3.0	167.5	180	30
Mesoporous anatase TiO_2 nanospheres/graphene composites	1.0–3.0	168	199	100
Porous TiO_2/C nanocomposite shells	1.0–3.0	335	171	330
TiO_2/graphene nanostructured composite	1.0–3.0	167.5	180	100
Carbon–TiO_2 composite (TC400)	0.9–3.0	75	153	30
Porous TiO_2 microsphere/RGO composite	1.0–3.0	168	180	100
TiO_2 and reduced graphene oxide nanocomposite	0.01–3.0	100	200	100
TiO_2–CNT sponges	0.0–3.0	100	210	100
Mesoporous TiO_2 nanocrystals grown in situ on graphene aerogels	1.0–3.0	100	200	50
Mesoporous TiO_2/graphene/mesoporous TiO_2 sandwich-like nanosheets	1.0–3.0	20	237	100
Ultrafine TiO_2 nanoparticles embedded in N-doped graphene networks (UTO/NGF)	1.0–3.0	168	165	200
		840	143	
Carbon-coated mesoporous TiO_2 nanocrystals grown on graphene	1.0–3.0	200	110	100
Hollow TiO_2/graphitic carbon spheres	1.2-2.5	100	178	100
		1000	137	1000
TiO_2/GO nanocomposite (SP20)	1.0–3.0	336	150	50
Ultra small TiO_2 nanoparticles in situ growth on graphene hybrid	0.0–3.0	100	186.6	100
Randomly oriented carbon-supported ultra-thin anatase TiO_2	1.0–3.0	170	172	100

1.4 Electrospinning

Electrospinning is an efficient method aiming to produce continuous nanofibers in a variety of ranges from submicron diameters down to nanometer diameters by using a high potential electric field [30].

Electrospinning technique has a broad spectrum of the applications in various fields from composites, filtration, biomedical applications, electronic devises, and most importantly, energy-related applications (fuel cell, batteries, supercapacitors, and solar cells) [17]. The main

advantages of this technique include easy assembly and operation, low cost, and ability to be scaled-up [14].

Generally, the electrospinning process is done by the assistance of solution which possesses molecular dipole moment. When the electric field is generated, due to the bipolarity of these molecules, the ink tries to become fibers as shown in Figure 1-6 [31]. As shown, when the electric field overcomes the surface tension of the ink, adjacent to the jet, a funneled flow creates a cone resulting in the fibers by subsequent evaporation of the assistant solution. This cone shape flow is called Taylor Cone and it is essential to be created to obtain a decent electrospinning process [30].

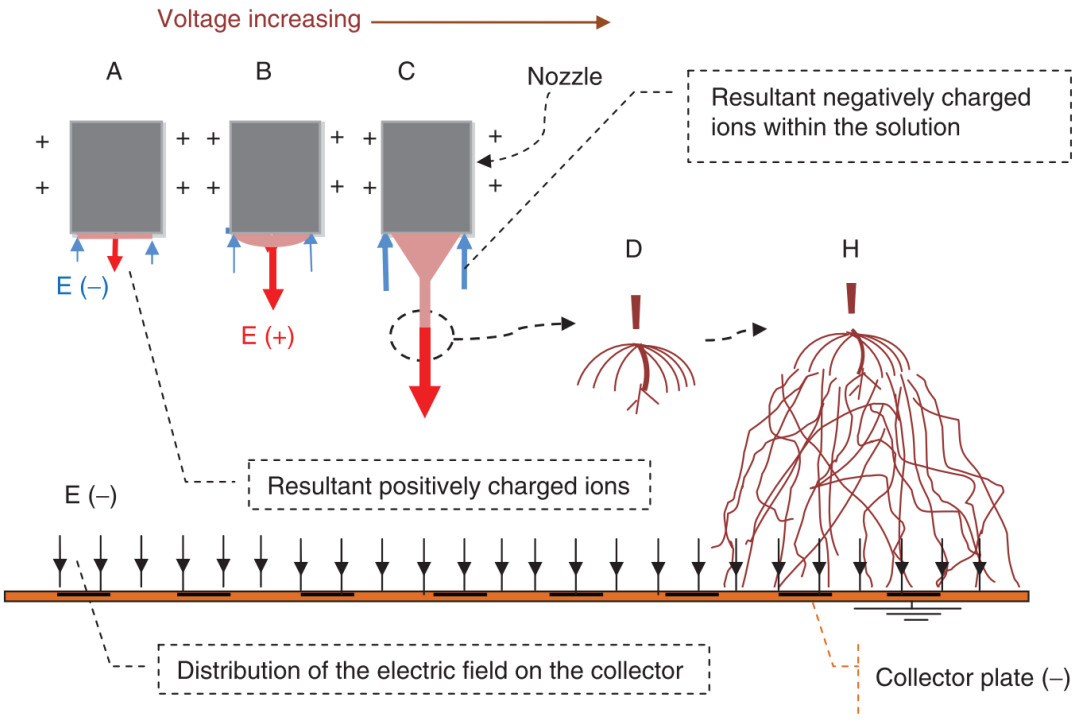

Figure 1-6. Electrospinning steps of the ink by increasing the voltage [19, 31].

1.4.1 Electrospinning Parameters

In order to obtain bead-free and uniform fibrous structure, there are some parameters required to be optimized. These parameters are divided in three main groups including solution parameters (viscosity, molecular weight, surface tension, conductivity, and solution properties), operation parameters (applied electric field intensity, feeding rate, needle to collector distance), and ambient parameters (temperature and humidity) [30]. Table 1-2 shows the impacts of the various mentioned parameters on the different structural morphologies [32].

Table 1-2. Electrospinning parameters impact on the fiber morphology [32].

Process parameter	*Effect on fiber morphology*
Viscosity/concentration	• Low concentrations/viscosities yielded defects in the form of beads and junctions; increasing concentration/viscosity reduced the defects • Fiber diameters increased with increasing concentration/viscosity
Conductivity/solution charge density	• Increasing the conductivity aided in the production of uniform bead-free fibers • Higher conductivities yielded smaller fibers in general (exceptions were PAA and polyamide-6)
Surface tension	• No conclusive link established between surface tension and fiber morphology
Polymer molecular weight	• Increasing molecular weight reduced the number of beads and droplets
Dipole moment and dielectric constant	• Successful spinning occurred in solvents with a high dielectric constant
Flow rate	• Lower flow rates yielded fibers with smaller diameters • High flow rates produced fibers that were not dry upon reaching the collector
Field strength/voltage	• At too high voltage, beading was observed • Correlation between voltage and fiber diameter was ambiguous
Distance between tip and collector	• A minimum distance was required to obtain dried fibers • At distances either too close or too far, beading was observed
Needle tip design	• Using a coaxial, 2-capillary spinneret, hollow fibers were produced • Multiple needle tips were employed to increase throughput
Collector composition and geometry	• Smoother fibers resulted from metal collectors; more porous fiber structure was obtained using porous collectors • Aligned fibers were obtained using a conductive frame, rotating drum, or a wheel-like bobbin collector • Yarns and braided fibers were also obtained
Ambient parameters	• Increased temperature caused a decrease in solution viscosity, resulting in smaller fibers • Increasing humidity resulted in the appearance of circular pores on the fibers

It is worthy to note that the reviewed research has been focused on the polymer solution. However, the present study required adding more parameters to the already-complicated system.

Besides optimizing the polymer solution concentration (PRS) in Eq. (1-4), addition of solid contents (TiO_2 and CB) which are insoluble in the polymer solvents are needed to be investigated by parameters like: Ink final solid ratio (ISR) in Eq. (1-5), dispersion concentration in Eq. (1-6), and finally the Polymer/CB/ TiO_2 ratio. The optimization process will be elaborated on the next chapter.

$$PRS = \frac{m_{polymer\ powder}}{m_{solvent} + m_{polymer\ powder}} \times 100 \quad (1\text{-}4)$$

$$ISR = \frac{m_{polymer\ powder} + m_{TiO_2} + m_{CB}}{Ink\ weight} \times 100 \quad (1\text{-}5)$$

$$Dispersion\ concentration = \frac{m_{CB} + m_{TiO2}}{m_{CB} + m_{TiO2} + dispersant} \quad (1\text{-}6)$$

1.5 Electrospun Electrode

In spite of the considerable achievements developing the gravimetric capacity of the LIBs, there are limitations over improving the areal capacities of anode materials [33]. For instance, high gravimetric capacities are obtained using Si due to the high theoretical capacities (3579 mAh/g), however, in terms of areal capacities, Si does not show considerable capacity [34] (see Figure 1-7).

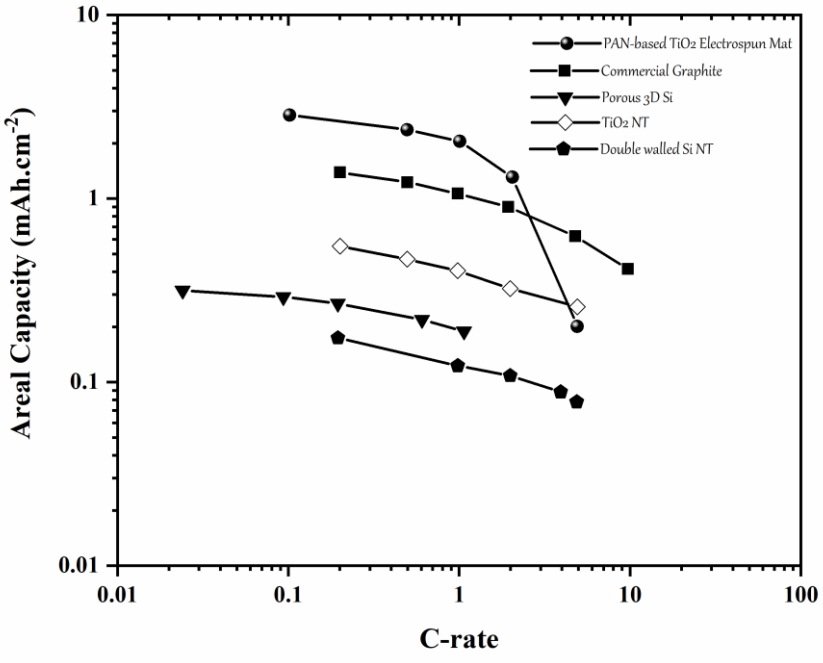

Figure 1-7. Areal capacity of different anode within various C-rates [34].

Electrospun anodes due to the good infiltration of the electrode to the increase of the contact surface between the electrolyte and active materials can improve the Li^+ transference. Moreover, the intra- and inter void within the fibers also intensify the efficiency of the electrochemical kinetics [34], accordingly the superior areal capacity can be achieved.

Taking advantages of electrospun structures, plenty of research have been done using different polymers in LIBs. Table 1-3 illustrates the advantages and disadvantages of the mentioned polymers, separately.

Table 1-3. Polymer used in the LIBs and their properties.

Polymer	**Polymer unit**	**Properties**	**Conductivity (S cm^{-1})**	**Ref.**
PVDF	CH_2CF_2	Strong electron withdrawing group (presence of -C-F), Chemical and Mechanical stability, High dielectric constant, High humidity absorption	insulator	[35]
PEO	CH_2CH_2O	Relative low conductivity, Low degree of dissociation	10^{-8}-10^{-3}	[36]
PMMA	$CH_2C(Me)(CO_2Me)$	Good conductivity, Poor mechanical properties	10^{-3}-10^{-2}	[37]
PAN	$CH_2CH(CN)$	Good conductivity, syneresis of solvent molecules	10^{-3}-10^{-2}	[37]

Among these well studied polymers, PEO by obtaining a potential to reach higher conductivities ($\sim 10^{-3}$ S.cm^{-1}), good electrospinning abilities, and remarkable mechanical properties grabs more attention as well [36]. However, due to the protic nature of this polymer and presence of $LiPF_6$ within the electrolyte, there are always concerns about the hydrolyze reaction of the solvated salt and polymer back bone [10]. Subsequently, thereby dissociation of the electrolyte, resulted HF could have a detrimental impact on the electrode performance both in negative and positive sides [10]. This side effect can be even be intensified by impact of the tendency of the ether functional group of the PEO in absorbing more cation ions (Li^+) which again impedes theses ions transfer as well [38].

1.5.1 PEDOT:PSS

As previously mentioned, the conductivity of PEO could be improved and one of the well-known methods is adding plasticizer to increase the degree of amorphous phase within the polymer, which is responsible for the conductivity. Another process to reach acceptable conductivity is adding other polymers like alkyl based low weight polymers [38]. The best result out of these processes doesn't exceed $\sim 10^{-3}$ S.cm^{-1}; hence, present study aims to offer even better solution to this barrier.

Among the family of the conductive polymers, poly(3,4ethylenedioxythiophene):poly (styrene sulfonate) (PEDOT:PSS) has superior properties like flexibility and being portable [39] (see Figure 1-8). The conductivity of this material is up to 0.2 S cm^{-1}. Even though, poor mechanical properties besides the difficulty to continuous deposition in the nonpolar surfaces are the weak point of this material [15, 40].

PEDOT:PSS is a polymer mixture of two ionomers, PSS and PEDOT, respectively. The first one is made up from a sodium polystyrene sulfonate, in which the sulfonyl group lost its proton and possessed a negative charge. The later (PEDOT) is a conjugated polymer and carries positive charges [41]. Thereby adding PSS, the conductivity of PEDOT decreases; however, the major reason for this addition is to make more stable water suspension due to the solubility of PSS in water [42].

Regarding the disadvantages of this polymer, it was reported that PEO (Poly(ethylene oxide)) as a carrier polymer can improve the poor rheological properties PEDOT:PSS, mostly a low viscosity, require using carrier polymers to process it [25, 43]. Even though the conductivity of the ultimate mixture will be reduced, thereby reaching a compromise, an acceptable conductivity is obtainable. Besides good electrospinning properties of the polymer and acceptable conductivity, the major reason for adding PEO to the structure is to avoid chain entanglement in the ultimate mixture compared to the other possible alternatives [44].

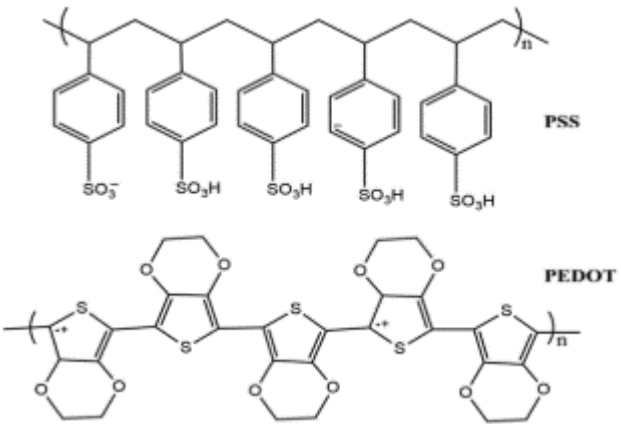

Figure 1-8. Structure of the PEDOT:PSS [45].

Additionally, this polymer shows the electrochemical activity as a supercapacitor in Ref. [46]. Therefore, using this polymer not only can escalate the conductivity, but it can improve the capacity of the anode as well.

1.6 Objective of this work

The rapid depletion of the confided fossil fuels and side effects of the using of them on the environment is one of the major problems in recent decades. Therefore, finding an alternative renewable energy resource is one of the hottest topics among the scientists. One of the promising energy systems for generating and, also storage of the energy is electrochemical system. Since 1970s, LIBs have gradually become an intrinsic part of the human being in modern civilization. Nowadays, it is undeniable that not only do almost every electronic device use LIBs, but the giant car industries commercialized their products based on these batteries as well. In response to the ever-increasing consumption of the LIBs, designing a best assembly of the cathode, anode, and electrolyte is of crucial significance. Graphite anodes due to abundance, good cyclability, and cost have targeted the battery industry, however, the poor safety and low performance in fast charge/discharge have struggled the researchers to find new alternatives. TiO_2 among the other anodes can compensate the disadvantages of the graphite anodes. Even though, the low conductivity of this ceramic impedes the full productivity of this material; therefore, presence of a conductive agent is highly required. In comparison of research done up to now, the Si anodes due to the high intrinsic capacity of Si possessed the highest gravimetric capacities. However, the anodes with this component lacks high performance in areal capacities since the high loading of this material was avoided due to the high expansion

in lithiation process (400%). Electrospinning technique is a promising solution to increase the areal capacity of the anodes by increasing the gross contact of the active material with electrolyte and facile Li^+ transportation. As a result, there is a number research done considering various active materials (CB, TiO_2, and Si) using different carrier polymers (PAN, PAA, PVDF and PEO). Accordingly, the higher conductivity of the polymer will result in better properties of the resulted anode. Among the conductive polymers, PEDOT:PSS possesses a relatively high conductivity; furthermore, it obtains electrochemical activity within the voltage suitable for TiO_2 (1-3 V). To our best knowledge, there is no similar research done aiming to use PEDOT:PSS as carrier for the electrospun anodes. This research was planned to produce TiO_2/PEDOT:PSS-based electrospun anode to take the full advantage of conductivity and electrochemical activity of the polymer besides safety and high rate performance of TiO_2 to achieve both gravimetric and areal capacity simultaneously.

Chapter 2. Experiments

The Experimental procedure was performed aiming to get a full coverage of solid contents on the fibers which includes two optimizing steps: i) PEO/PEDOT:PSS ratio, ii) PEO/PEDOT:PSS/CB/TiO_2.

2.1 Materials

For the electrospinning part in this project, the utilized materials include TiO_2 (anatase), CB (carbon black), and PEO (polyethylene oxide) powders; and solvents comprise DMF (N,N-Dimethylformamide) and distilled water. PEDOT:PSS suspension, TiO_2 and PEO powders were bought from Sigma Aldrich Co. DMF solution (purity of $>$ 99.9 %) is bought from Merck company.

2.2 Ink preparation procedure

2.2.1 Carrier Solution Preparation

To prepare the carrier solution, PEO polymer powder was weighed using a balance, then distilled water was added to the powder (see Scheme 2-1).

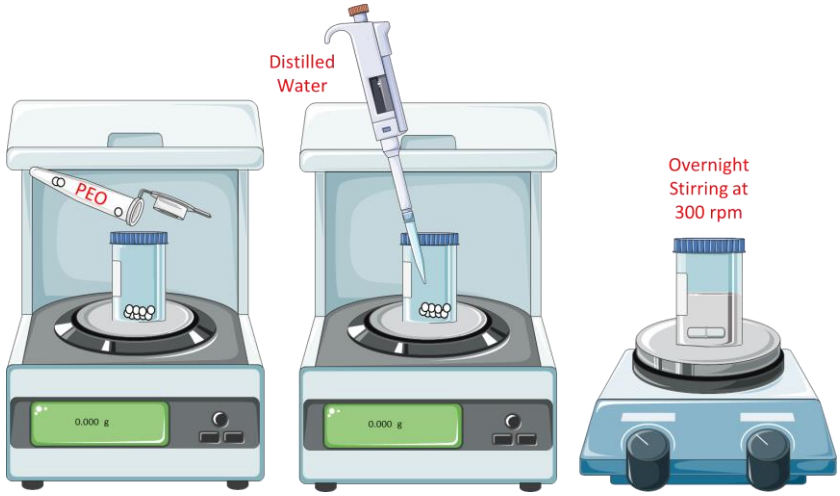

Scheme 2-1- PEO solution preparation procedure: weighing of PEO powder (left), addition of solvents (middle), and stirring overnight by an agitator (right).

In order to add the conductive agent, after preparation of the PEO solution, PEDOT:PSS was added to the very solution. After an hour, the color of the suspension becomes dark blue. To get a decent homogeneous mixture, the mixture was stirred at 100 rpm for overnight (See Scheme 2-2).

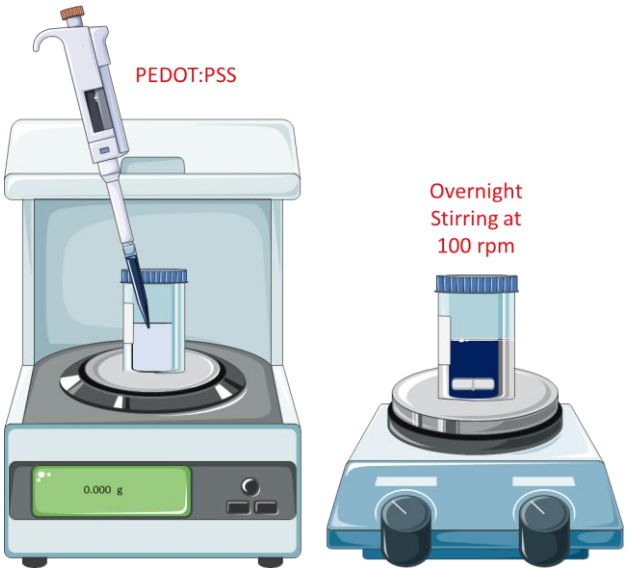

Scheme 2-2- PEDOT:PSS addition to the solution and stirring aiming to get uniform dispersion.

Since the PEDOT:PSS suspension has a constant polymer content, the concentration of the this polymer was kept constant up to the end of the experiments. In the following, Table 2-1 shows the amount of the variables which were tested. To be easily followed, PEO/PEDOT:PSS ratio in this project entitled as PR.

Table 2-1. Different variables to obtain the suitable electrospinnable ink.

Experiment name	PR	PEO Solid Ratio (%)	Mixture polymer Ratio (%)
Set 1	1	2	1.5
	1	2	3
	1	2	4.5
Set 2	2	2	1.5
	2	2	3
	2	2	4.5

2.2.2 Solid Suspension Preparation

As received TiO_2 powder was weighed and poured into the vial. Water was added subsequently (Scheme 2-3a). In order to disperse the powders within the solvent homogeneously, the suspension was put into the ultrasonic bath for 1 hour (Scheme 2-3b). Carbon black, as a supportive material aiding the conductivity, was added to the suspension besides the DMF (Scheme 2-3c). Finally, another 1-hour ultrasonic bath was performed to obtain a uniform dispersion (Scheme 2-3d).

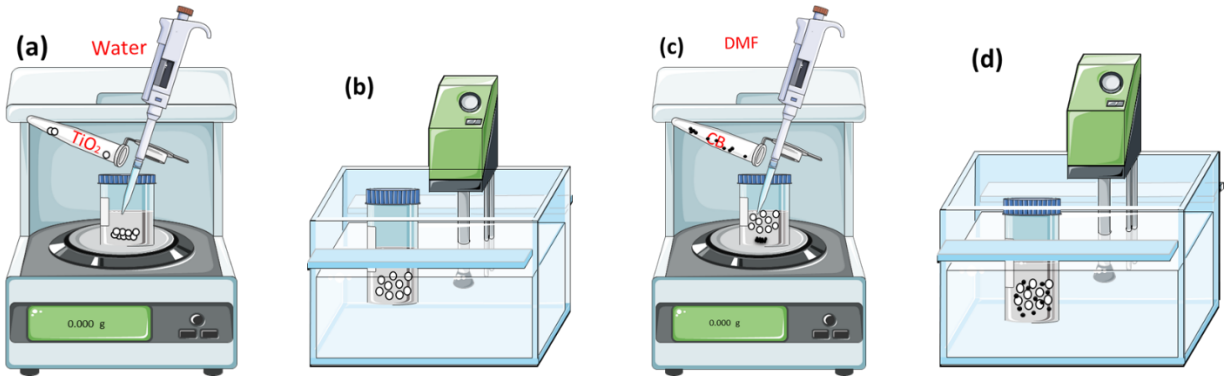

Scheme 2-3. Solid solution preparation procedure: a) TiO_2 weighing and addition of water, b) dispersion of TiO_2 in water, c) addition of carbon black and 2nd solvent (DMF), and d) dispersion of carbon black within the solution.

2.2.3 Final Ink Preparation

Thereby adding the already-prepared polymer solution to the suspension using a syringe, the ink for the electrospinning procedure was obtained. In order to guarantee the uniform dispersion of the powders into the carrier, the ink was stirred at 600 rpm for overnight (see Scheme 2-4).

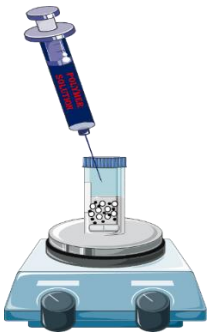

Scheme 2-4. Addition of polymer solution into the dispersed solid solution.

Finding best possible ink for the decent solid coverage (CB & TiO_2) on the electrospun matrix of PEDOT:PSS requires modifying lots of parameters including PR, ink final solid ratio, molecular weight of the used polymer, and the ratio of the solvents (DMF/Water) besides the operational parameters like applied voltage, relative humidity, and flow rate. For the sake of simplicity, the weight ratio of TiO_2, CB, and polymer is kept as 70/20/10. In the experiments chapter, all these parameters were elaborated on.

2.3 Electrospinning

In order to get good fibers, the operating parameters play a significant role in the electrospinning procedure. Usually, feeding rate, voltage, and the distance between the needle and the collector is of great importance. However, the electrospinning machine used in this project possesses the ability to control the humidity (see Scheme 2-5). Therefore, the parameters under control exceeds to four.

Considering the experiment possibilities, literally, there are at least 96 experiments should be done to optimize the conditions. Following the experiments procedure, it was understood that some parameters did not affect the procedure notably; as a result, the number of experiments was declined, the details are elaborated in the results section.

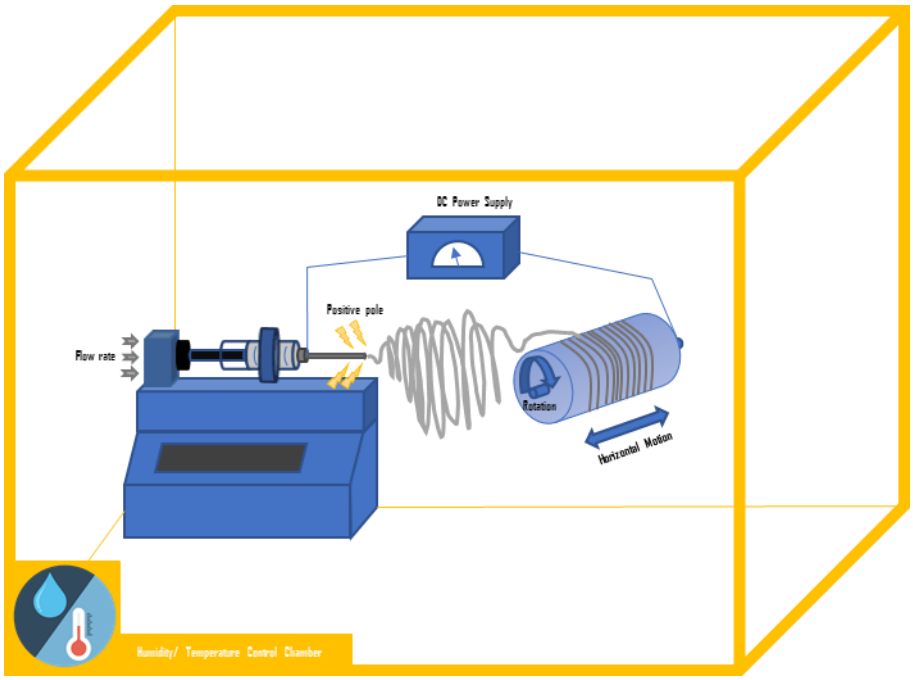

Scheme 2-5. Electrospinning setup used in this project. It includes the chamber for humidity and temperature monitoring.

After achieving the suitable electrospun matrix, the matrix was gently pealed from the aluminum foil (see Figure 2-1), then, using a hydraulic press machine, the electrodes were compacted at 0.5-0.6 ton for 5 minutes. Afterwards, they were cut using a punching die with a punch diameter of 1.5 cm. The electrodes then were dried using vacuum oven at 60℃ overnight. Avoiding the humidity absorption of the electrodes, after weighing the electrodes, they were transferred to the glow box for assembling.

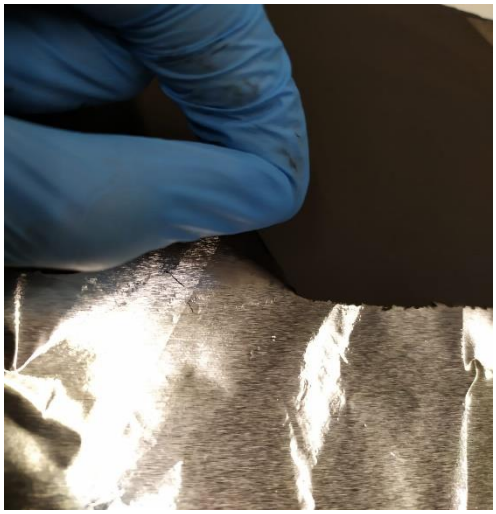

Figure 2-1. Pealing the electrospun matrix from the aluminum foil.

2.4 Electrode Assembly

Anode cells were prepared using 2032 coin cells to examine the electrochemical properties of the electrospun matrix. The assembling of the cells was done under a pure-argon-filled glove box (GP CAMPUS, Jacomex). Figure 2-2 shows the components of the LIBs. Since in this study only a half cell was investigated, instead of the anode and cathode, Li foil and electrospun matrix were used respectively.

Li chip was used as the counter electrode, and the solution of 1 M LiPF6 in ethylene carbonate (EC) and dimethyl carbonate (DMC) (1:1 (v/v)) was utilized as the electrolyte. A Celgrad 2400 film was used as the separator.

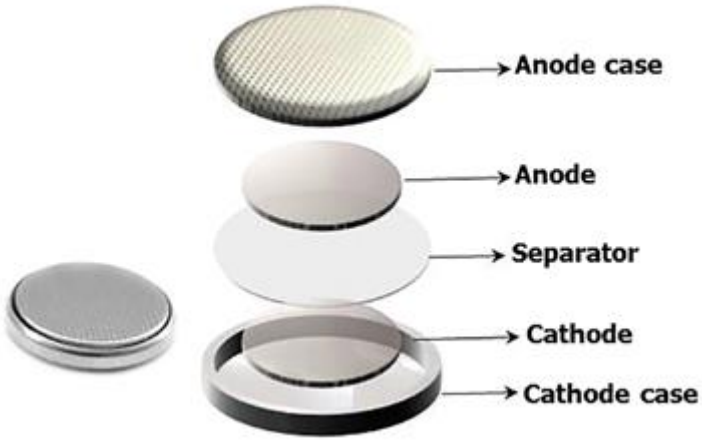

Figure 2-2. Assembly of the coin cell [9].

2.5 Characterization

2.5.1 SEM

In order to thorough study of the optimum condition for electrospinning process, the quality of the resulted fibers, parameters affecting the fibers diameter electrospun matrix, initial materials particle size, and the quality of the coverage of the samples, field emission scanning electron microscopy (FE-SEM) (Zeiss Leo Supra 35VP SEM-FEG) at a working voltage of 3 kV was used.

2.5.2 RAMAN Spectroscopy

Raman spectroscopy is a technique generally used to investigate the vibrational modes of molecules to identify the structural composition of the materials. The basic idea of using this device is analyzing of the peak shift of the incident beam (a monochromatic light source) after being scattered due to the different inelastic scattering of photons by the various vibrational modes within the molecular structures [45]. For data acquisition, Nd-YAG laser with a power of 0.5 mW at 532 nm was used and the spectral range covered 5 cm^{-1} to 2000 cm^{-1}.

2.5.3 XRD

X-ray powder diffraction is a fast technique used to study of the parameters related to the unit cells in the materials' structure including unit cell diameter, the atomic planes, dislocations density, and cell size. Thereby using a monochrome X-ray with a known wavelength and fitting into the Bragg equation ($\lambda = 2dsin(\theta)$), each plane within the structure can diffract and give a characteristic peak within a specific degree of a rotating goniometer

($\lambda, d, and\ \theta\ represents$ wavelength of the incident beam, atomic distance, diffraction angle, respectively). Therefore, the existing atomic planes can be detected accordingly.

In this study, X-ray diffraction analysis (XRD; Bruker AXS GmbH D8 Advance) was used to detect the phase composition and crystal structure of materials. The tests were performed at 2θs ranging 5-90° and step size of 0.01 using Cu-Kα 1.5406 Å radiation.

Thereby analyzing the pattern and comparing of the resulted electrodes with the initial materials, the difference in the cell size and the atomic distances were studied. In order to get the average cell size, Debye-Scherrer equation ($D = K\lambda/\beta Cos(\theta)$) was used, in which K is a constant number, and β shows the line broadening at half the maximum intensity (FWHM) of each diffracted peak [47].

2.5.4 TGA

Thermogravimetric analysis (TGA) is a method which measures the mass of sample over time by changing the temperature. By comparing the input mass with a reference crucible, different reactions (decomposition, phase transition, oxidation, etc.) within the experiments' temperature range can be detected. In this research, in order to calculate the mass of inorganic active material within the electrode, the electrospun electrodes was analyzed by Shimadzu DTG-60 thermal analyzer at the rate of 10°C/min up to 1400°C under air atmosphere.

2.5.5 FTIR

Fourier-transform infrared spectroscopy (FTIR) is a simple technique aiming to measure the absorption or emission of the infrared spectrum in contact with a liquid, solid, and gas. The absorbance or transmittance within the specific wavelength range can be used to the identify the atomic bonds in the structure of the analyzed material [51]. In this research, the FTIR measurements were carried out using Bruker Equinox 55 equipment in the range of 500–4000 cm^{-1}.

2.5.6 Electrochemical analysis

In order to investigate the electrode performance considering different current densities, the Galvanostatic Charge/Discharge test are usually performed. In this method, the assembled cell is investigated under the constant current within a specific voltage range by a repetitive sequence of charge/rest/discharge/rest. The utilized charge/discharge current is often measured by C-rate, which is relative to the maximum theoretical capacity of the active material used within the electrode, for instance, 1C shows the necessary current applied or drained from the battery to reach a complete charged or discharged state in one hour. 1C represents 335 mA/g

for the anatase [50]. In this research, the prepared cells were put into galvanostatic cycling test using MTI 8-channel battery analyzer from 1 V to 3 V (vs. Li/Li^+) at 0.1 C for 100 cycles. For the measuring of the rate capability, the assembled cells were tested by the current density order of 0.1C, 0.5C, 1C, 2C, and 0.1C for 5 cycles at every step.

Cyclic voltammetry test is a potentiodynamic electrochemical measurement in which the potential of working electrode is ramped by time, and after reaching a specific potential, the potential will be decreased reaching initial potential. By repeating this test to a desired number of cycles, a plot displaying the variation of current created within the working electrode vs. the implied potential can be depicted [21]. Thereby performing this test, useful information about presence of redox reactions and the reversibility of the electrochemical reactions can be achieved. In this study, PARSTAT MC system was used to get a cyclic voltammetry test (CV) at a scan rate of 0.1 mV/s in a potential window of 1–3 V vs. Li/Li^+. Electrochemical impedance test (EIS) was also done at a range of 100 mHz to 100 kHz using the constant potential of 10 mV.

Chapter 3. Results and Discussion

As previously mentioned, the main objective of this project is preparing an electrospun matrix with the fully covered fibers. Therefore, the major struggle of this project was dedicated to optimizing the condition for electrospinning. In the second part, the received matrix was assembled and tested as an anode in coin cell form.

3.1 Initial Materials Characterization

XRD patterns of TiO_2 and CB are shown a complete anatase phase as shown in Figure 3-1. Both patterns are consistent with the literature [48, 49]. As-received TiO_2 obtaining Anatase phase possessed a tetragonal structure with 101, 112, 200, 105,211, 204, 116, 220, and 215 high intensity planes and 2θ of 37, 48, 53, 55, 62, 68, 70, and 75, respectively.

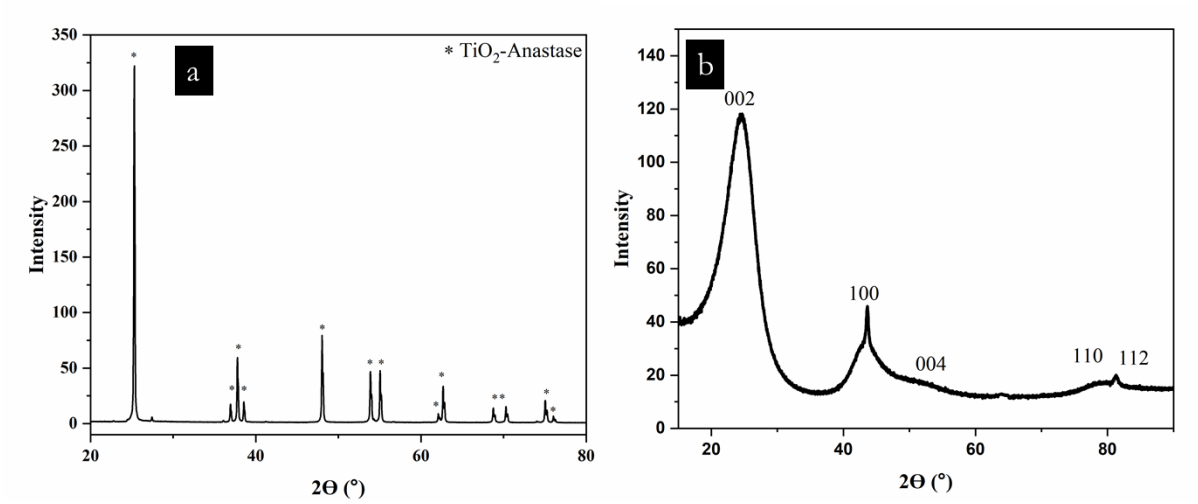

Figure 3-1. XRD pattern for the initial materials: (a) commercial anatase, and (b) CB.

FTIR patterns of the PEO powder and PEDOT:PSS solutions are shown in Figure 3-2. Characteristic peaks within the pattern indicated in the figure are extracted from Refs. [51] and [52]. Due to the different bending modes (twisting, scissoring, wagging, and rocking), a complicated pattern of the FTIR existed for the $-CH_2$ bonds. The related peaks are also shown within a table in the same figure.

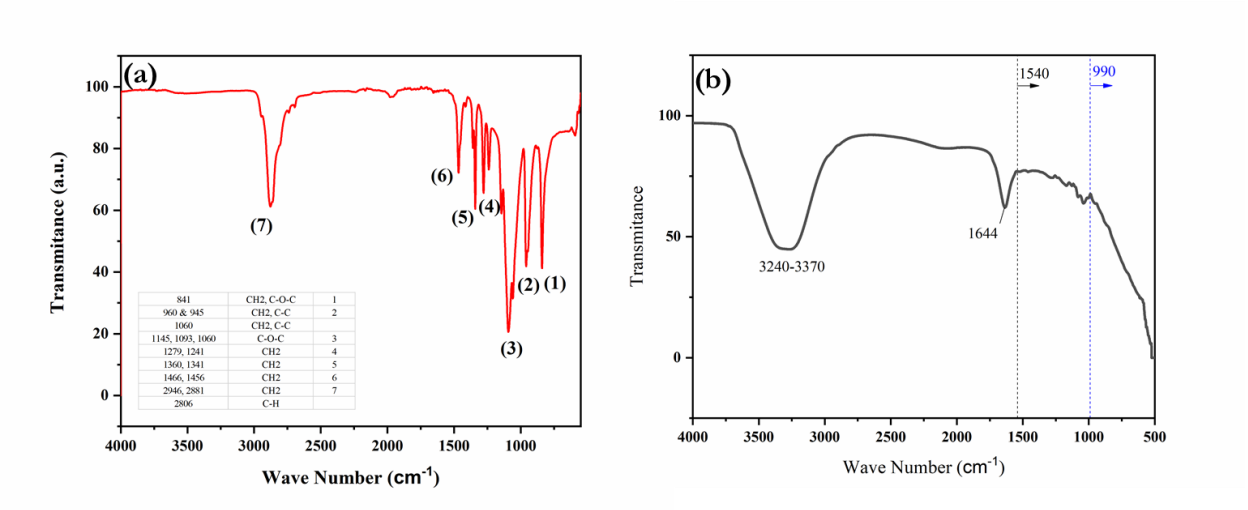

Figure 3-2. FTIR patterns for (a) PEO powder and (b) PEDOT:PSS suspension in water.

The FTIR spectrum of the PEDOT:PSS polymer includes 3353, 1644, 1644,1540-890, 990-690 cm^{-1} for C-H bond, C=O bond, Ethylenedioxy group, Thiophen ring, and C-S bond vibration, respectively [52] .

Figure 3-3 shows the SEM image of the as-received anatase powders. The particle size is less than 200 nm.

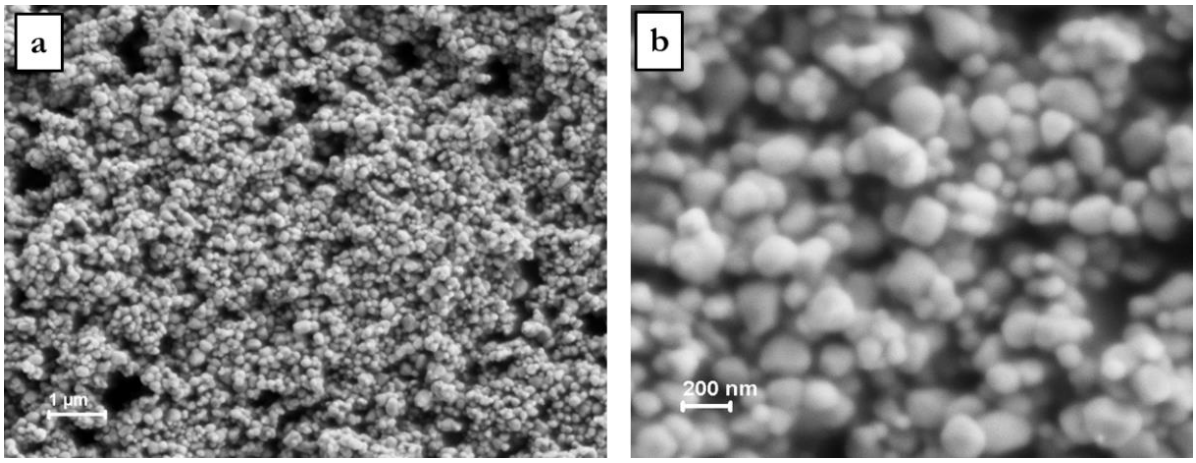

Figure 3-3. SEM picture of as-received anatase powder in two different magnifications.

3.2 Optimizing PEO/PEDOT:PSS Electrospun Matrix

In order to get fibers out of the PEO/PEDOT:PSS solution, Set 1 and Set 2 experiments were carried out, and the results are shown in Table 3-1. As shown, since the PEDOT:PSS is hard to electrospun by itself, adding similar amount of PEO (PR=1) didn't help the electrospinning process even in various polymer mixture ratios. In order to extract good fibers out of the solution, the amount of the PEO was doubled and in 2nd set of experiments there is a sign of fibers in the 1.5% solid ratio; however, it possessed some droplets on that as well (see Figure 3-4).

Table 3-1. Result of the electrospinning process for the PEO/PEDOT:PSS solution.

Experiment name	**PR**	**PEO Solid Ratio (%)**	**Mixture polymer Ratio (%)**	**Results**
Set 1	1	2	1.5	Sprayed
	1	2	3	Sprayed
	1	2	4.5	Sprayed
Set 2	2	2	1.5	Fibers + droplets
	2	2	3	Fibers
	2	2	4.5	Sprayed

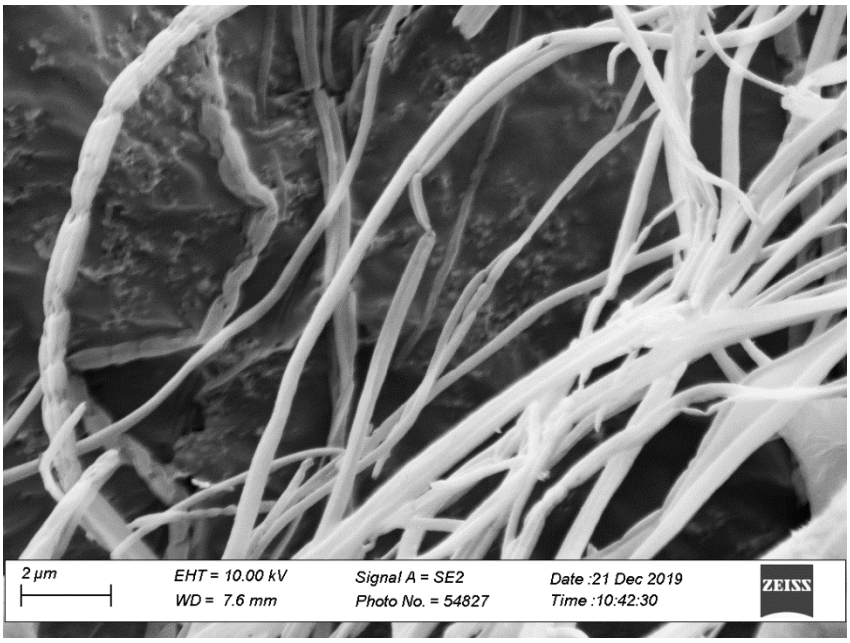

Figure 3-4. Electrospun fibers out of PEO/PEDOT:PSS solution: Polymer Mixture solid ratio is 1.5% PR=2.

Thereby decreasing the water amount, nice fibers out of the solution becomes possible. Figure 3-5 shows the fibers electrospun with the polymer mixture solid ratio of 3%. Additionally, the fibers can be easily pealed out of the Al foil since the extra solvent does not exist anymore. The average diameter obtained from SEM image is 231 nm, and a relatively wide range of diameters are obtained from this process.

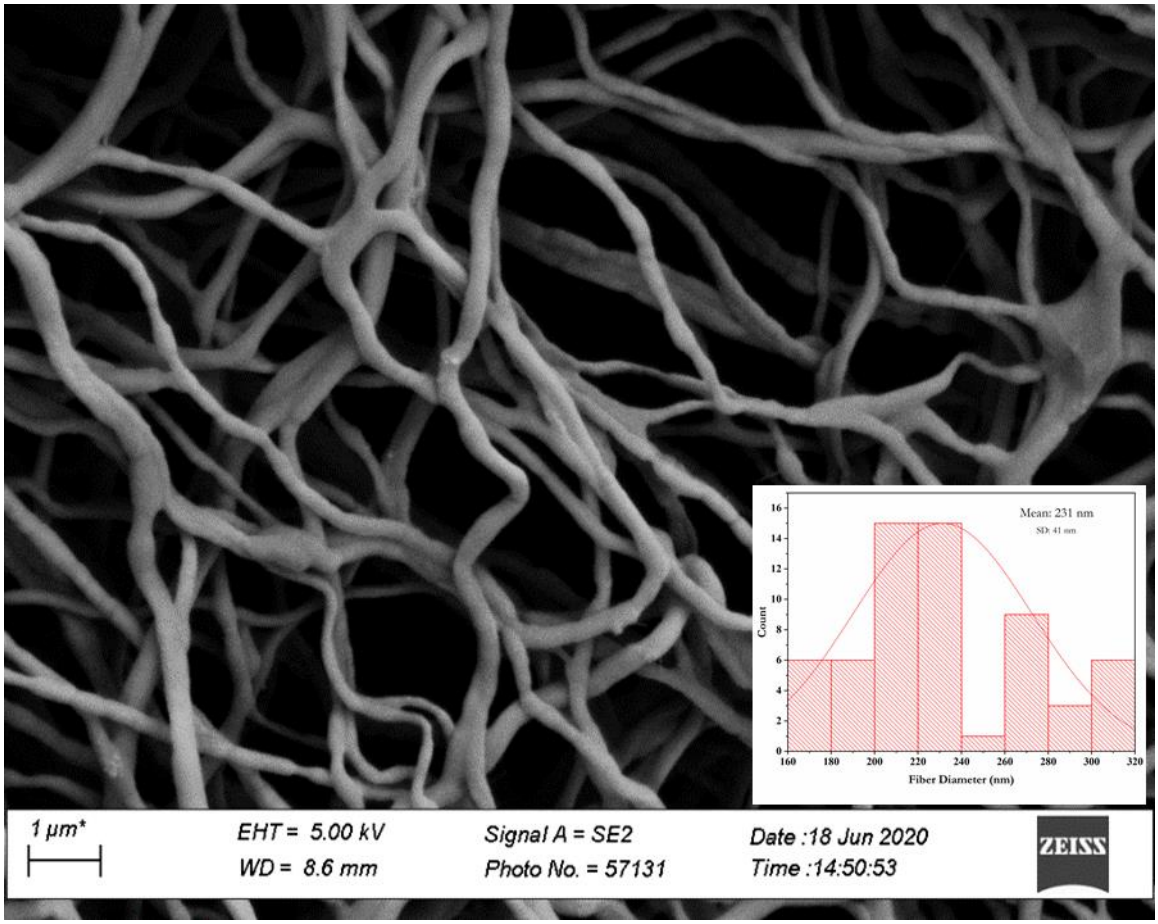

Figure 3-5. Electrospun fibers out of PEO/PEDOT: PSS solution: Polymer Mixture solid ratio is 3% PR=2.

3.3 Optimizing TiO_2/CB/Polymer Electrospun Matrix

Afterwards, TiO_2 and CB were added to the solution. Aiming to achieve the highest capacity ever, the amount of the active material should be the highest possible amount. According to the research done so far, the optimum properties have been obtained when the weight ratio of the contents is kept as TiO_2/CB/Polymer:70/20/10 [15 & [53][54]. Therefore, these ratios were kept constant through out the experiments.

In the following, the effect of dominant parameters was elaborated on separately.

3.3.1 Effect of Operation Parameters

After several trials and errors, it was observed that decent electrospinning condition was achieved in humidifies less than 30%. For simplicity, the distance of the needle to the collector and drum speed were kept constant for whole the experiments as 12 cm and 200 rpm, respectively. Fortunately, the overall behavior of the ink given the implied voltage and flow rate can be extended to the whole sets of the experiments. Figure 3-6 demonstrates the continuous operational parameters for the whole experiments, which 17-19 kV and 0.8 to 1.2 mL/h will be safe ranges for applied voltage and flow rate, respectively.

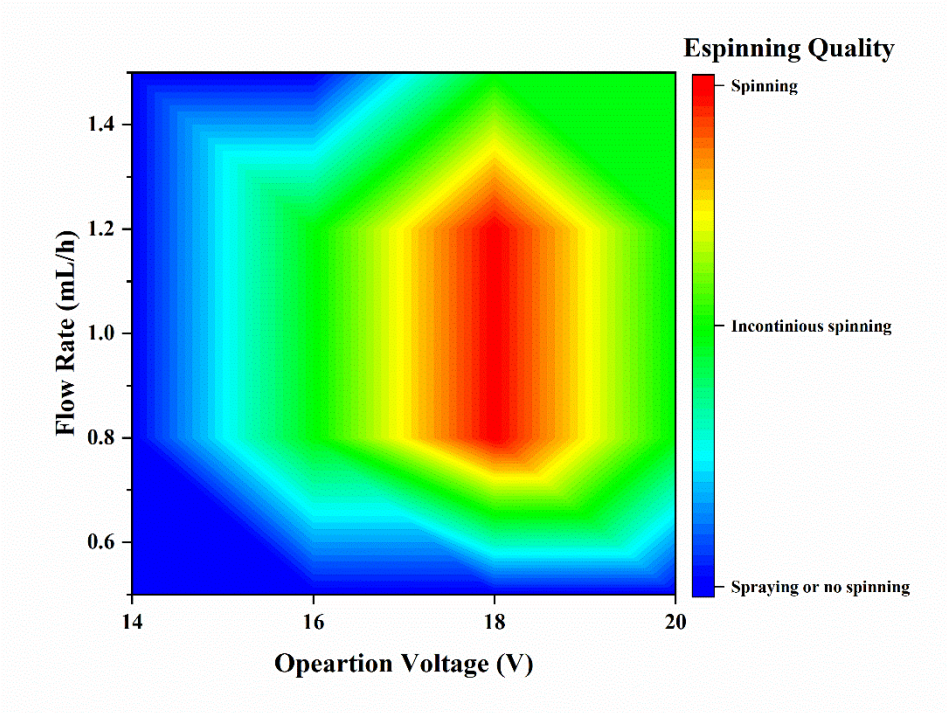

Figure 3-6. Effect of the operational voltage and flow rate on the quality of the electrospinning.

3.3.2 Effect of DMF/Water Ratio

The main reason for the addition of DMF to the ink is to reach a better dispersion of CB within the solution. Three sets of the experiment were conducted considering the weight ratio of DMF/Water 0, 0.2, and 1, separately. Given DMF/Water=0, CB powders couldn't disperse completely in the ink and it stuck to the magnet bar within the vial. As a result, the ratio of 0.2 and 1 were examined through the experiments.

Electrospinning results are shown in Table 3-2. As shown, disregarding the PEO solid ratio and ink solid ratio, all the experiments done with the weight ratio of the DMF/Water=1 resulted in spraying (Set 3). This phenomenon can be attributed to the high boiling temperature of DMF solvent which impedes the solvent evaporation before reaching the collector.

Table 3-2. Electrospinning results ink containing TiO_2/CB/Polymer.

Experiment Set	PEO Solid Ratio (%)	DMF/Water	Ink solid ratio (%)	Results	Related Figure
Set 3 (PR=1)	2	1	18 22	Sprayed	-
	5	1	18 22	Sprayed	-
	10	1	18 22	Sprayed	-
Set 4 (PR=2)	2	0.2	18 22	Fibers + Splashes	(Figure 3-7)
	10	0.2	18 22	Fiber (not fully covered)	(Figure 3-8)
Set 5 (PR=5)	2	0.2	18 22	Fibers (not fully covered)	(Figure 3-9)
	5	0.2	18 22	Fibers (fully covered)	(Figure 3-10) (Figure 3-11)
	10	0.2	18 22	Fibers (fully covered)	(Figure 3-12) (Figure 3-13)

3.3.3 Effect of PEO Solid Ratio

Inks with PEO solid ratio of less than 2% contains excess amount water. Accordingly, this results in spraying of the ink due to lack of sufficient evaporation during the electrospinning process. On the other side, inks with solid ratio of more than 10% became very viscous to suck with the syringes.

As shown in Figure 3-7, ink with PEO solid ratio of 2% and PR=2 in both 18 and 22% ink solid ratios contain splashes besides the fibers. Thereby increasing the PEO solid ratio to 10%, the nice fibers can be electrospun (see Figure 3-8). For, during the electrospinning, by increasing the viscosity of the polymer carrier, the uniformity of the fiber after building up the Taylor cone stays longer. However, the fibers are not fully covered with the powders as well.

For all sets of the experiments, the main reason which the ink solid ratios do not surpass 22% and decline from 18% is that the resulted fibers became splashed and sprayed, respectively.

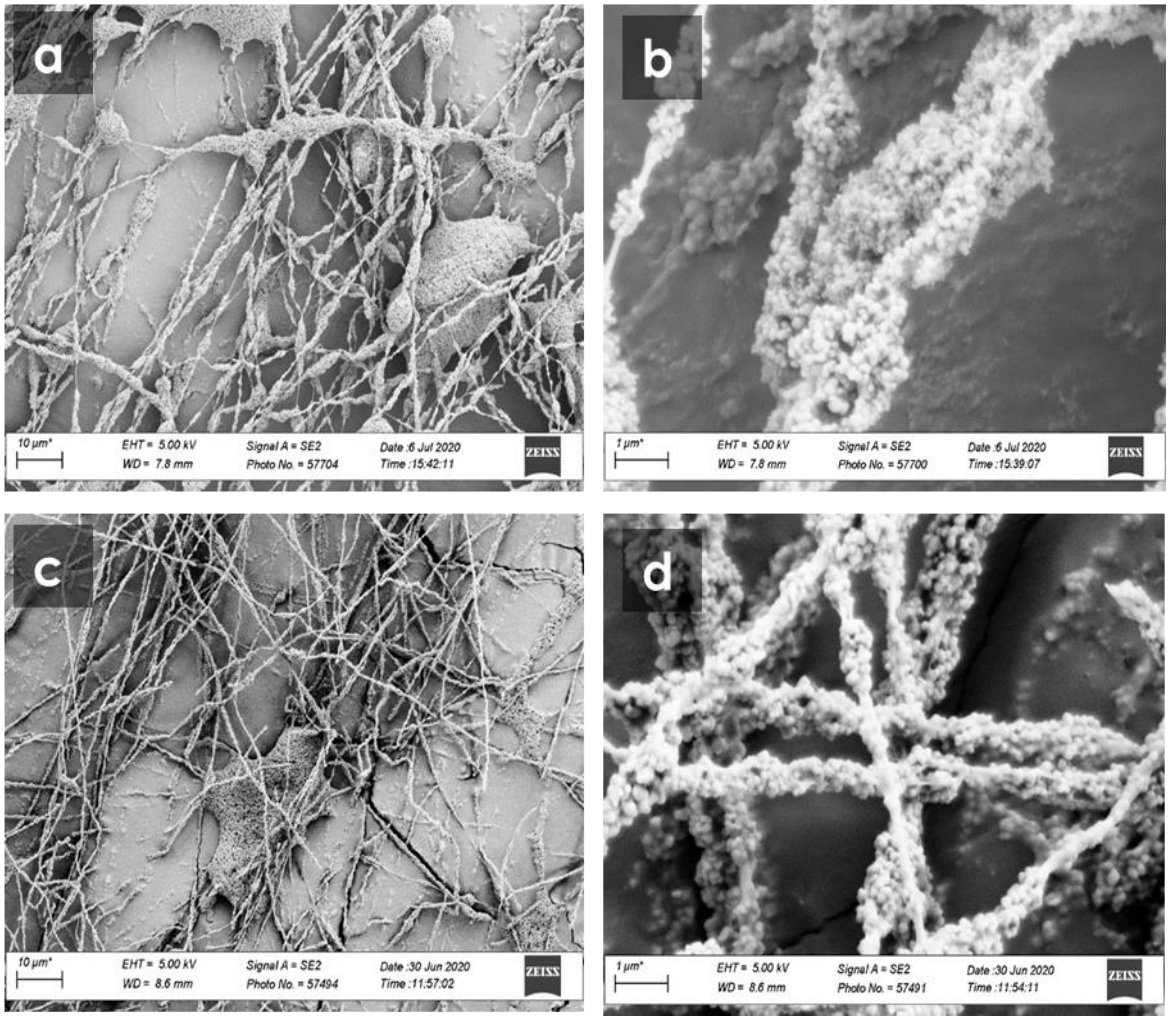

Figure 3-7. Electrospun matrix of TiO_2/CB/Polymer=70/20/10 with PEO solid ratio of 2% and PR=2: (a) and (b) 18 % ink solid ratio, (c) and (d) 22% ink solid ratio.

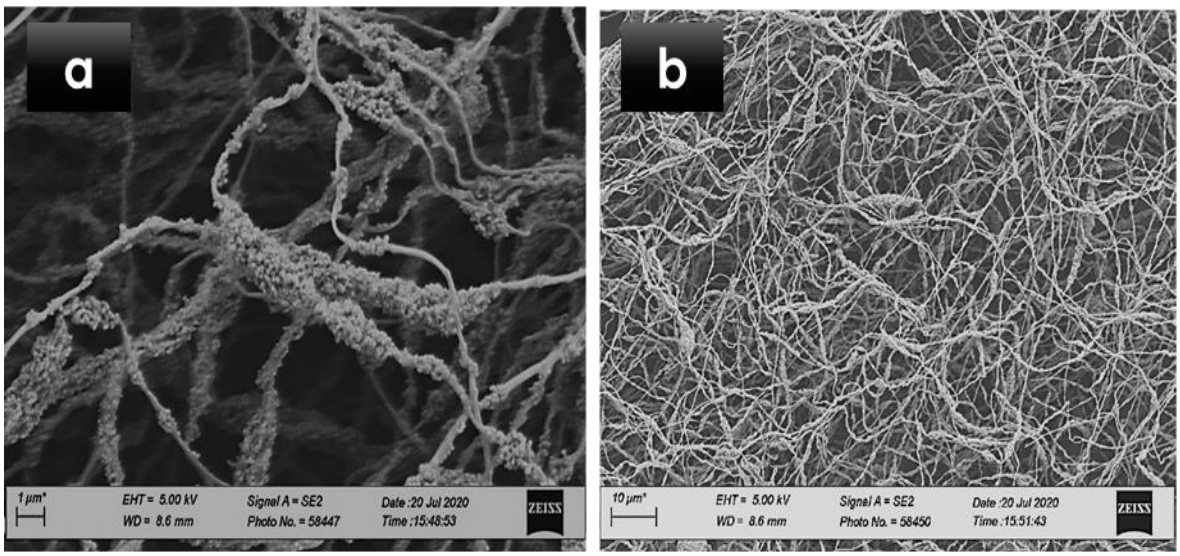

Figure 3-8. Electrospun matrix of TiO_2/CB/Polymer=70/20/10 with PEO solid ratio of 10% and PR=2 with 22% ink solid ratio.

3.3.4 Effect of PEO/PEDOT:PSS (PR)

Adding more PEO helps to increase the electrospinning process since it is one of the handy polymers which can become fiber in a wide range of humidities and electrospinning voltages. Even though, adding excess amount of the PEO will damage the conductivity of the ultimate matrix.

In Figure 3-9, thereby increasing the PR to 5, the better distribution of the solid particles can be observed. However, there are lots of not covered fibers as well. Same scenario happened to the higher ink solid ratios, 22%.

By increasing the PEO solid ratio to 5% and keeping PR as 5 (Figure 3-10 and Figure 3-11), the distribution of the particles becomes more uniform. Furthermore, the electrospun matrix with 22% ink solid ratio experienced fully coverage of the fibers and relatively the less particle agglomeration in the middle of the fibers, which means that the particles distribution becomes even more homogeneous.

Thereby further increasing the PEO solid ratio to 10%, decent distribution for the fibers became available. Figure 3-12 and Figure 3-13 shows the particles distribution on the fibers for two different ink solid ratios.

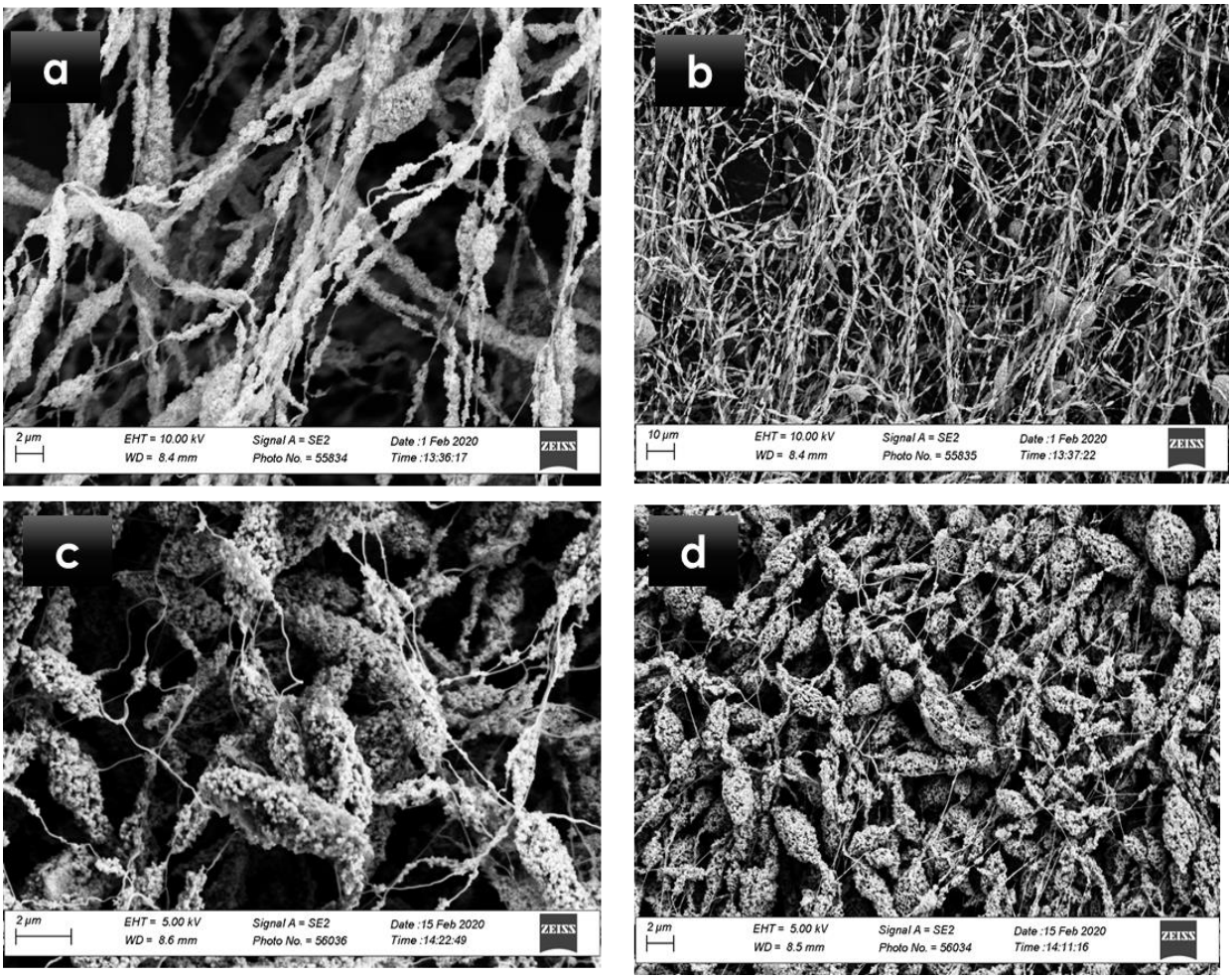

Figure 3-9. Electrospun matrix of TiO_2/CB/Polymer=70/20/10 with PEO solid ratio of 2% and PR=5: (a) and (b) 18 % ink solid ratio, (c) and (d) 22% ink solid ratio.

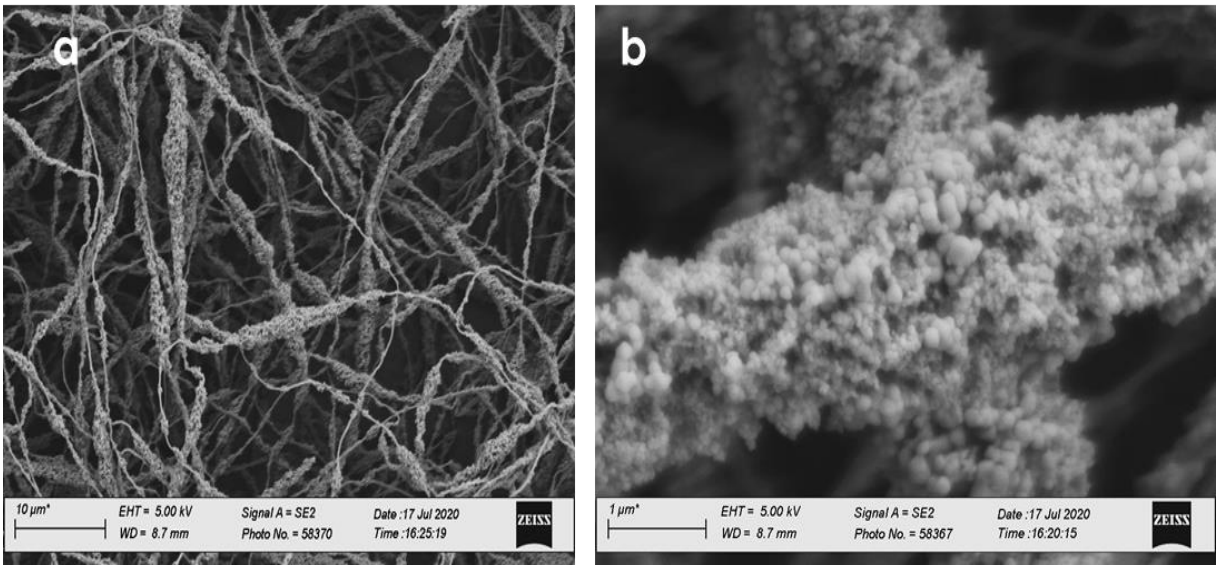

Figure 3-10. Electrospun matrix of TiO_2/CB/Polymer=70/20/10 with PEO solid ratio of 5% and PR=5: 18 % ink solid ratio.

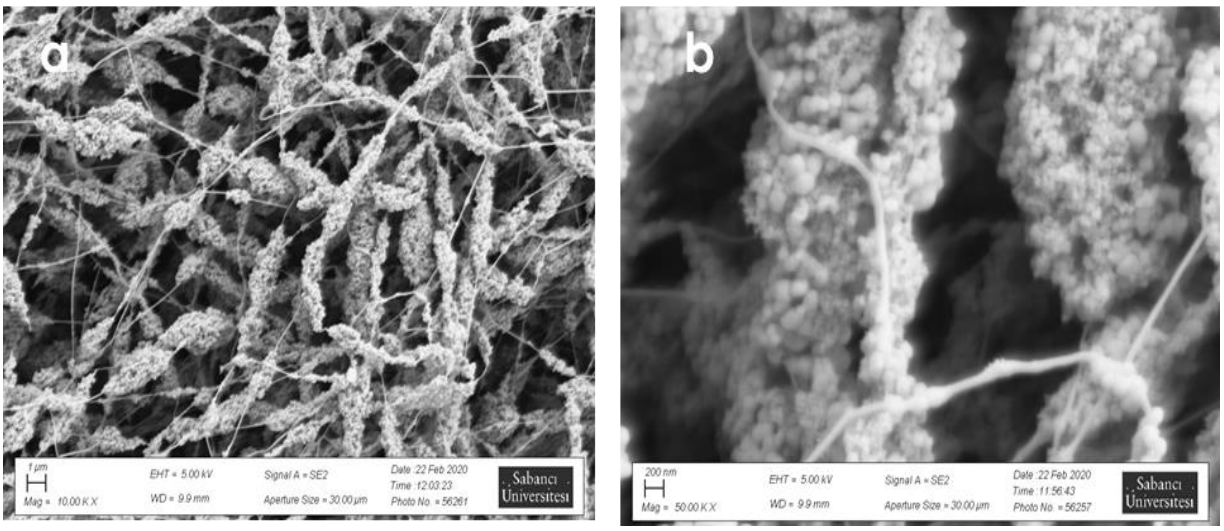

Figure 3-11. Electrospun matrix of TiO_2/CB/Polymer=70/20/10 with PEO solid ratio of 5% and PR=5: 22 % ink solid ratio.

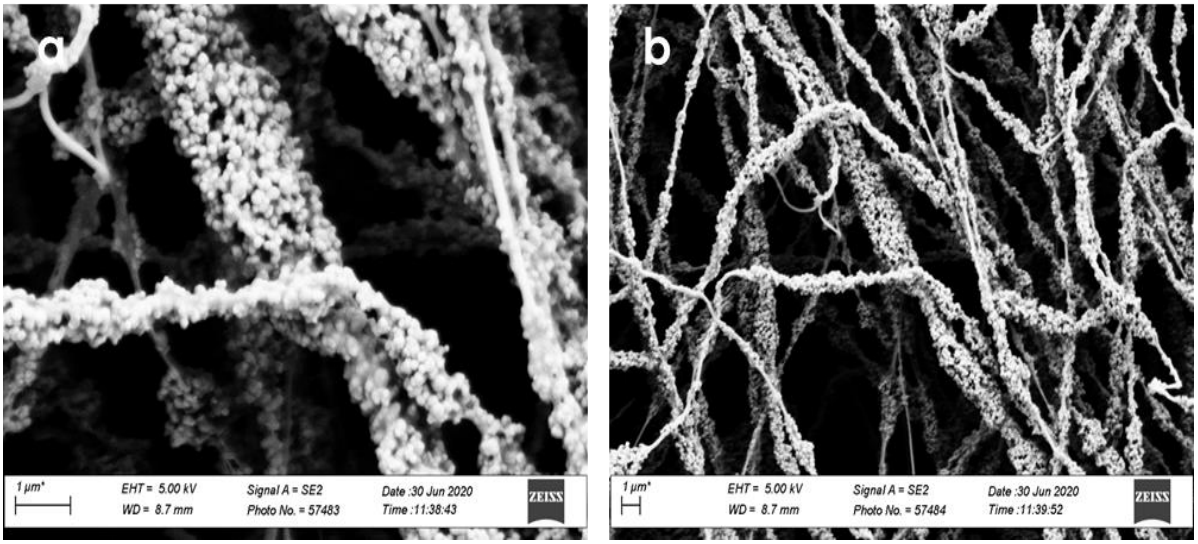

Figure 3-12. Electrospun matrix of TiO_2/CB/Polymer=70/20/10 with PEO solid ratio of 10% and PR=5: 18 % ink solid ratio.

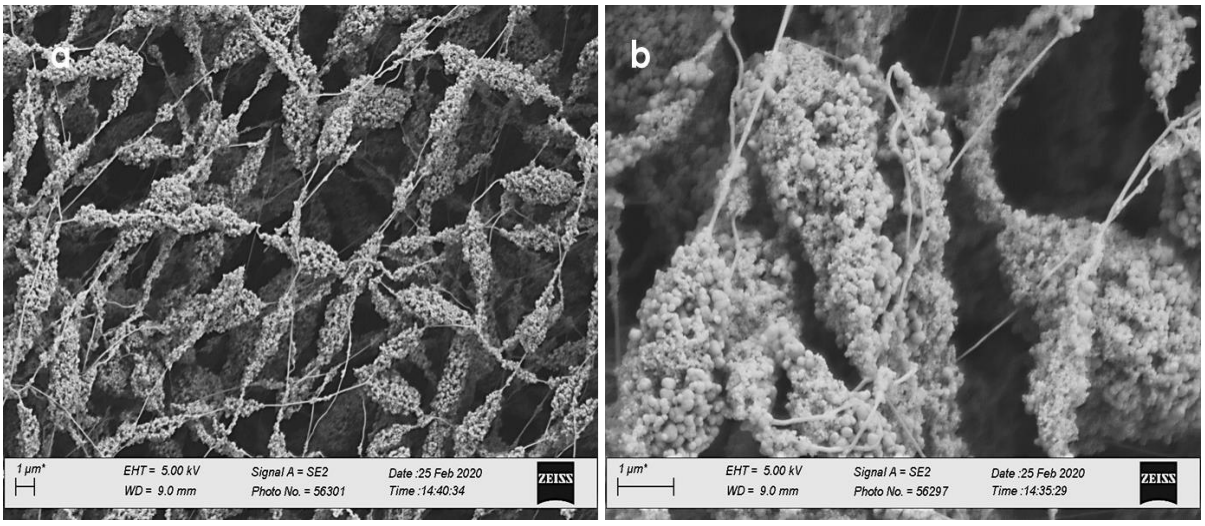

Figure 3-13. Electrospun matrix of TiO_2/CB/Polymer=70/20/10 with PEO solid ratio of 10% and PR=5: 22 % ink solid ratio.

3.3.5 Effect of PEO Molecular Weight

Thereby repeating the experiments for the PEO solid ratio of 10% with PR=5 (18%) with lower molecular weight, the fibers with high molecular weight resulted in better particle distribution (see Figure 3-14). According to the diameter distribution of the fibers, it can be understood that using higher molecular weight of the polymer resulted in the higher fiber diameters (841 vs. 562 nm) and since the particles are embedded within the polymeric structure, the higher diameter fibers can lead to better electrochemical performances. As a result, for the rest of the experiments, the high molecular weight PEO was used.

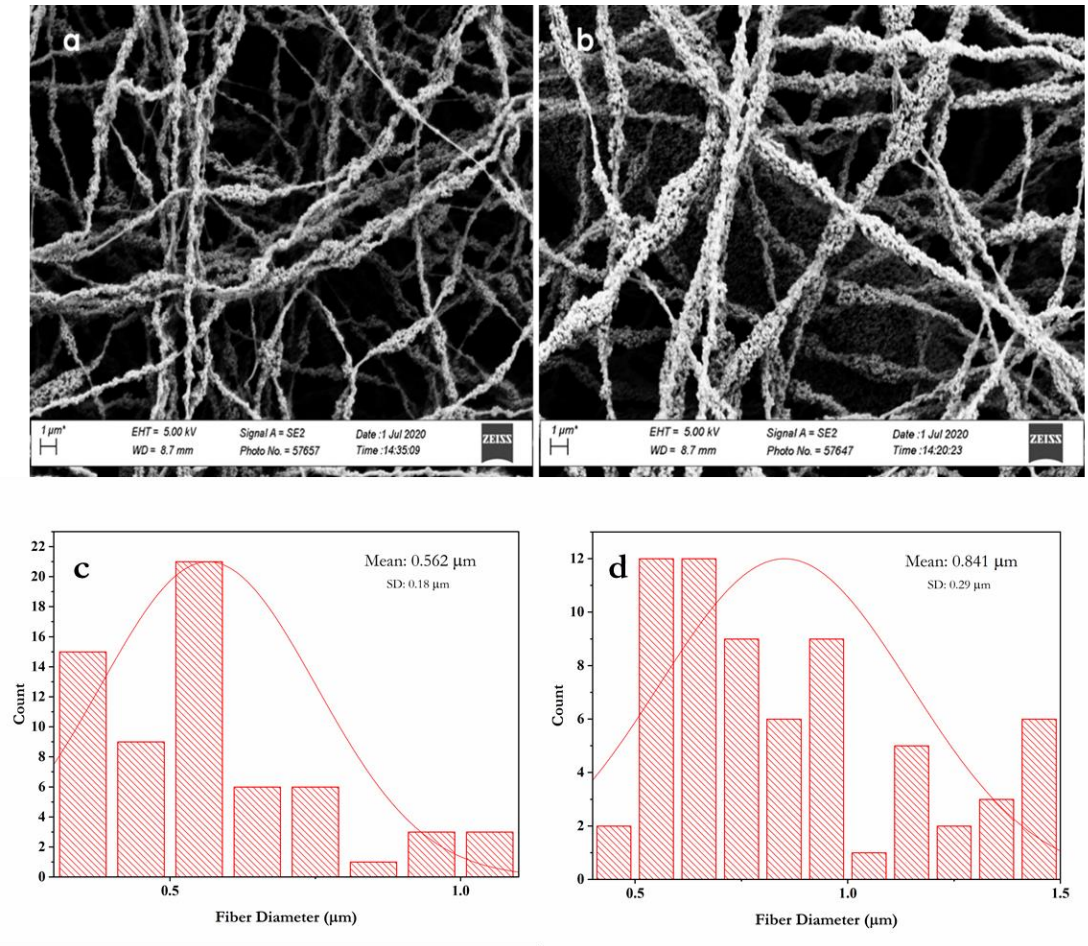

Figure 3-14. The effect of different molecular weights used PEO on the particle distribution: (a) low molecular wright and (b) high molecular weight in which (c) and (d) are the fiber diameter distribution diagrams, respectively.

3.3.6 Effect of Ink Solid Ratio

Generally, the fibers with high diameters (indicating better powder coverage) are desirable. Thereby increasing the ink solid ratio, the diameter of the fibers due to the increasing

the total ratio of the solid materials over the solvents increased. All the SEM images shown in Figure 3-9 to Figure 3-13 proves this claim. However, the main problem with the polymers with high ink solid ratio is the particle agglomeration after electrospinning. In the following, some strategies are considered to modify the agglomeration condition.

By increasing of the number of experiments to fully understand the behavior of electrospinning process, it comes out that the fully covered fibers are not obtainable unless PR becomes higher than 4 and ink solid ratio obtains some amount between 20-24% (Figure 3-15).

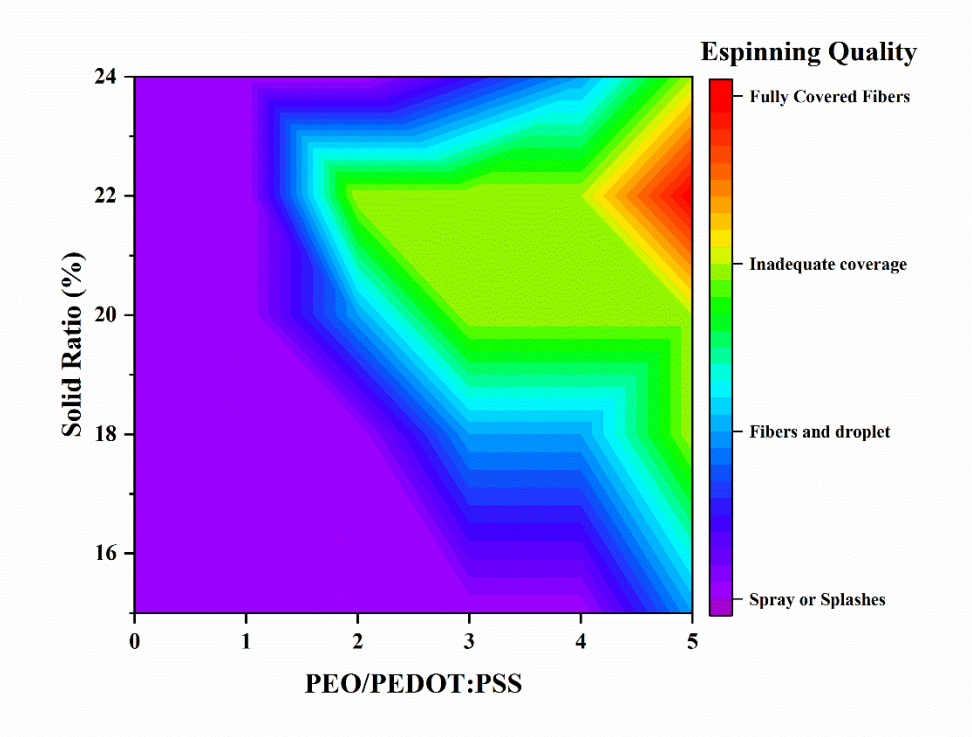

Figure 3-15. Simultaneous effect of the PR and ink solid ratio on the electrospinning process.

3.3.7 Effect of Ultrasound Vibration after Adding the Polymer to the Ink

In order to get a better distribution of the particles, the ink was put in the ultrasonic bath for 15 minutes and this resulted in more agglomerated particles (see Figure 3-16).

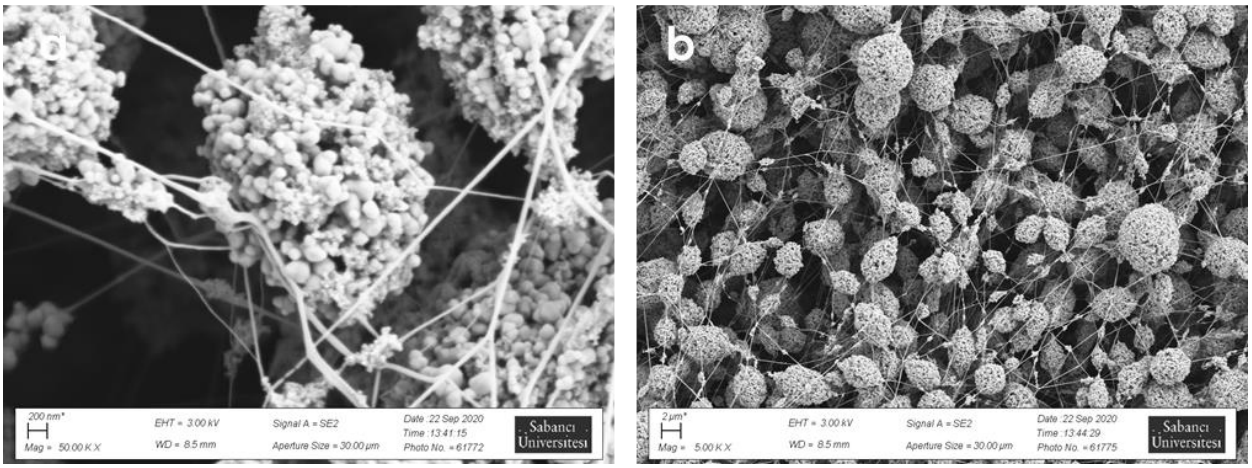

Figure 3-16. The effect of ultrasonic bath after polymer addition on the particle distribution.

3.3.8 Effect of Prob Sonication

Thereby introducing the prob sonication with amplitude of 2 for 15 minutes, solid dispersion becomes even better (see Figure 3-17). Especially for the case of higher ink solid ratios (see Figure 3-18).

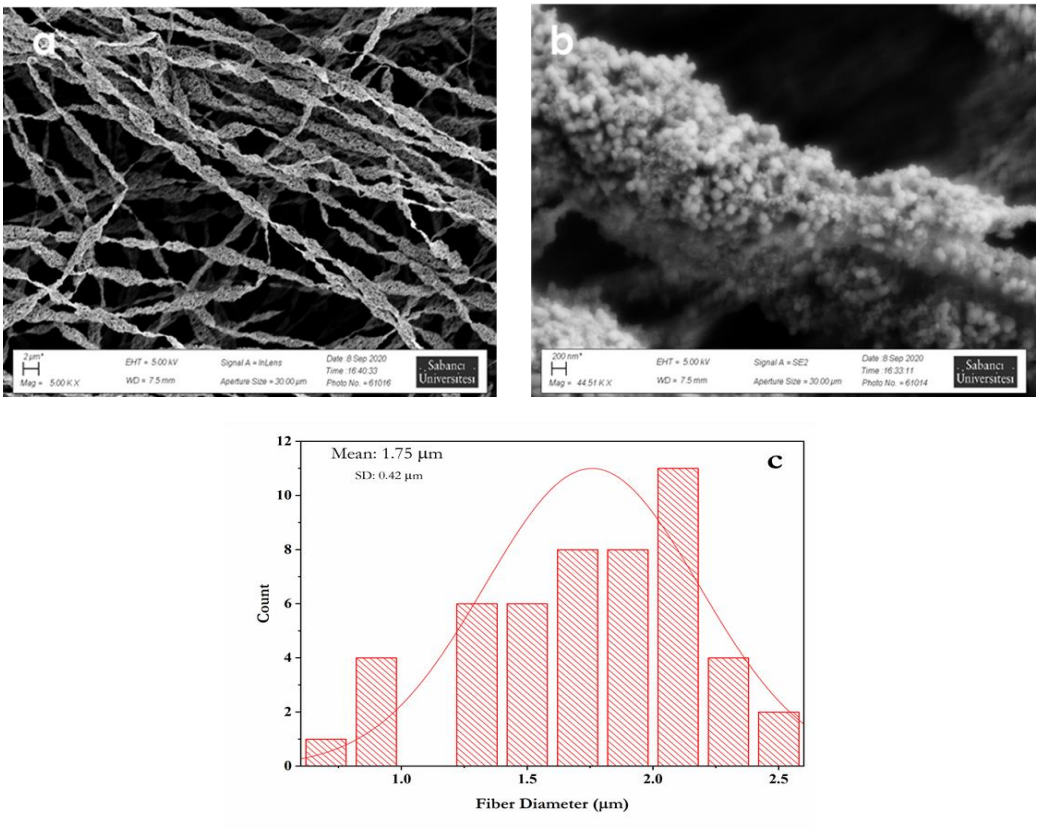

Figure 3-17. Effect of prob sonication for the electrospun matrix with PEO solid ratio of 10% and PR=5: 18 % ink solid ratio.

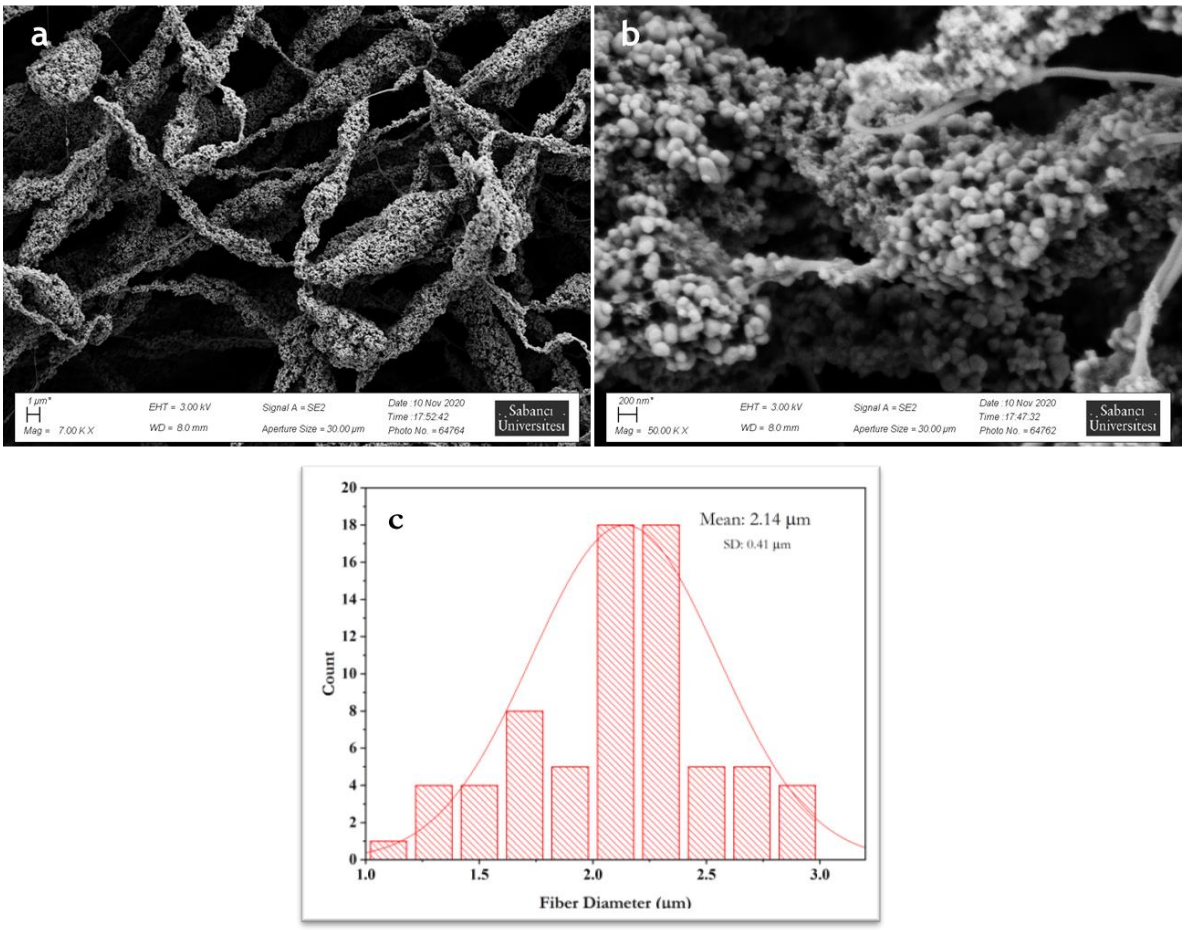

Figure 3-18. Effect of prob sonication for the electrospun matrix with PEO solid ratio of 10% and PR=5: 22 % ink solid ratio.

By comparing the fiber diameter distribution histograms of the prob sonicated samples, it can be understood that not only did the diameter become higher (2.14 vs. 1.75 μm) but more homogeneous structure with an acceptable average diameter was obtainable.

3.4 Characterization of the Electrospun Matrix

After optimizing the best electrospinning condition, the received mat was dried in vacuum oven at 60℃ overnight and put in the vacuum box for the other characterizations. For each of characterizations, the material was put on the test condition immediately after taking out of the vacuum to avoid the humidity effect on the samples. The final mat possessed 159 μm and 600 μm thicknesses, respectively.

3.4.1 TGA

The TGA test was carried out to determine the accuracy of the inorganic material added to the ink and remained within electrospun mat. The test was done under air flow up to 1400℃ to ensure the exact amount of the remaining inorganic material. Figure 3-19 shows the TGA analysis of the electrospun mat. The water content (less than 2%) was evaporated till 100℃ and up to 300 ℃ polymeric materials was burnt. Starting from 300℃ till 650℃, whole the carbon black was burnt. The remaining inorganic material is in a good match with what added to the ink (69.6913% vs. 70%).

This measurement will be used for the further calculation in the specific capacity of the material.

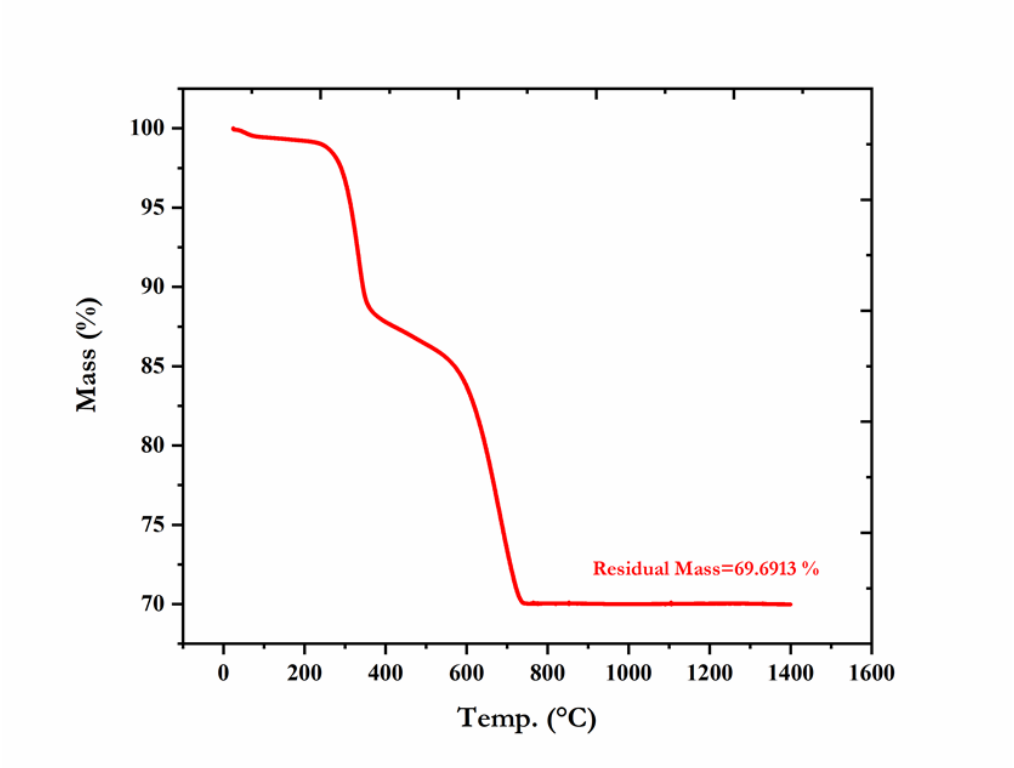

Figure 3-19. TGA analysis of the electrospun matrix under air atmosphere.

3.4.2 XRD

Figure 3-20 shows the XRD patterns of the as-received anatase powder compared with the electrospun mat. At the first glance, the intensity of the anatase peak was remarkably reduced due the less amount of the used powder. As expected, since the maximum material includes anatase (70% weight), the related peaks dominate within the pattern. A broad region

is because of the presence of both polymer and carbon black within the structure. The peak in 21.03° is related to the CB presence.

All the peaks within the structure experience a shift to the lower degrees, which proves the higher interplanar distance in the electrospun matrix. The calculated interplanar distance shows that the very amount was increased from 1.67 to 1.78 $\dot{A}$. Similar increase in the lattice spacing has been mentioned and attributed to the intercalation of the structure with tendency of the anatase atoms to make bond with the PEO molecules [55].

There is also a peak broadening exists in the XRD pattern. Thereby using the Debye-Scherrer equation, the particle size distribution was calculated using the characteristic peaks of the anatase. As a result, the particle size after electrospinning was decreased from 223 nm to 167 nm. Since the material's particles did not go through processes may result in particle size change, one possible description is presence of the amorphous material (PEO) within the structure causing peak broadening [47].

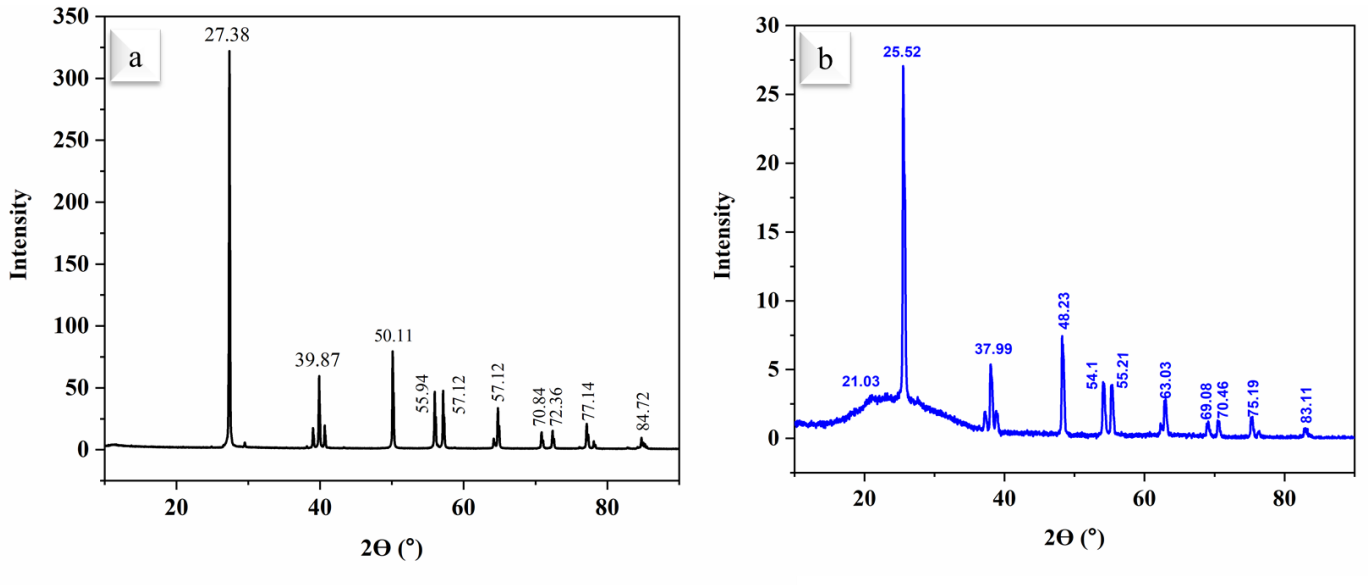

Figure 3-20. XRD patterns of (a) the initial anatase sample compared with (b) the electrospun matrix. The numbers on the peaks represent the diffraction angle for each peak.

3.4.3 FTIR

In order to ensure the presence of the polymer conductive agent (PEDOT:PSS) within the electrospun matrix, the FTIR test was carried out (Figure 3-21). Since most of the matrix comprises the anatase powder, it can dominate the other peaks within the matrix. Even though,

it is brought out that there is peak for SO_3H in PSS (1020 cm^{-1}) that exists even by the dominance of the TiO_2 peak. This peak can show that the polymer conductive agent is present after electrospinning process. Other peaks won't be detected due to the low intensity and low amount of the polymer in the electrospun matrix. The huge and wide peak related to the OH stretching within the range of 4000 to 3000 cm^{-1} was disappeared due to the water evaporation.

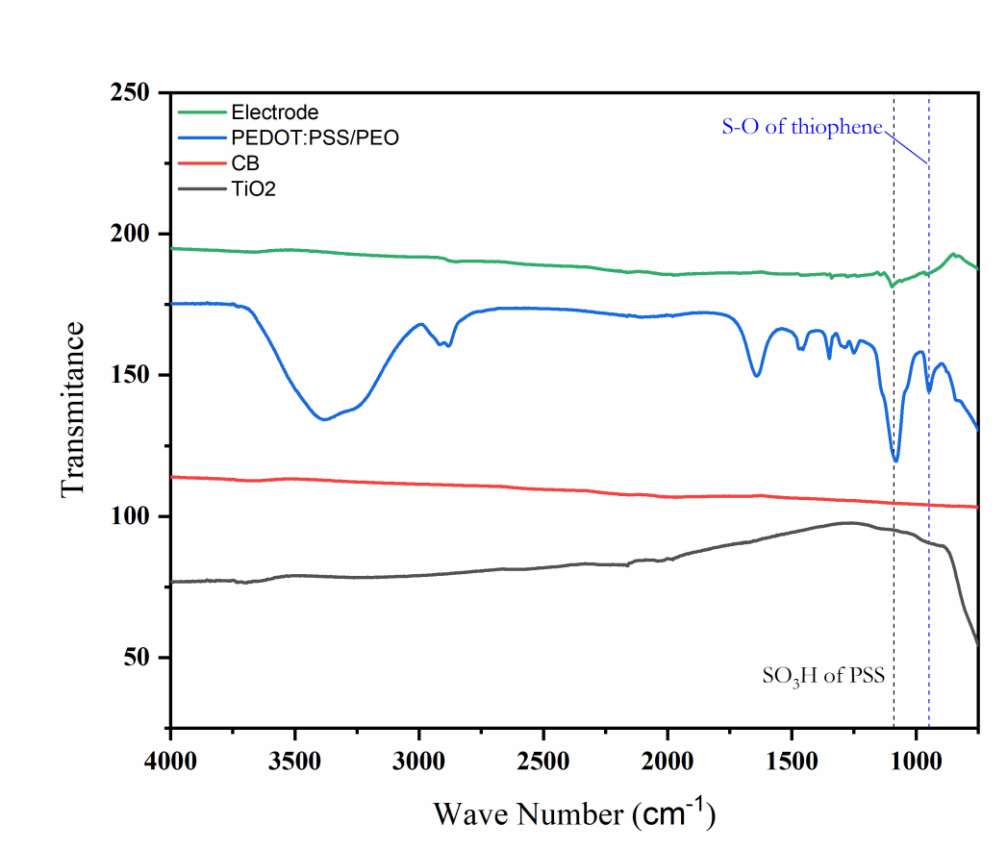

Figure 3-21. Comparison of the FTIR pattern of the component within the electrospun matrix with the initial materials.

3.4.4 RAMAN Spectroscopy

Pristine PEDOT:PSS/PEO, TiO_2, and CB are also investigated by Raman spectroscopy and the spectra is shown in Figure 3-22. The vibrational modes of PEDOT are placed at 1255, 1368, 1440, and 1506 cm^{-1} and assigned to the C_α─C_α inter-ring stretching, C_β─C_β stretching, C_α═C_β symmetrical, and C_α═C_β asymmetrical vibrations, respectively. The vibrational mode of PSS is located at 1568 cm^{-1}. The relative intensity of Raman scattering peaks for the treated films are intense and narrow [45].

Sharp peaks appeared in 146, 394, 512, and 637 cm^{-1} are assigned to E_g, A_{1g}, B_{1g}, and E_g vibrational modes, respectively [56]. Thanks to the presence of anatase in high amount, the impact of these peaks is visible in the electrode spectrum as well.

In comparison of the electrode with the initial materials, this is understood that most intensive peaks of the PEDOT:PSS in the pristine sample were not able to make impact on the electrode mat. In magnified box, two peaks of 1250-1450 and 1550-1660 cm^{-1} regarding D band (disorder band), G band (ordered band), respectively, shows the graphene band may exist in the CB. Due to very less amount of the added PEDOT:PSS, the trace of this polymer could be shown as an small back ground in the magnified box.

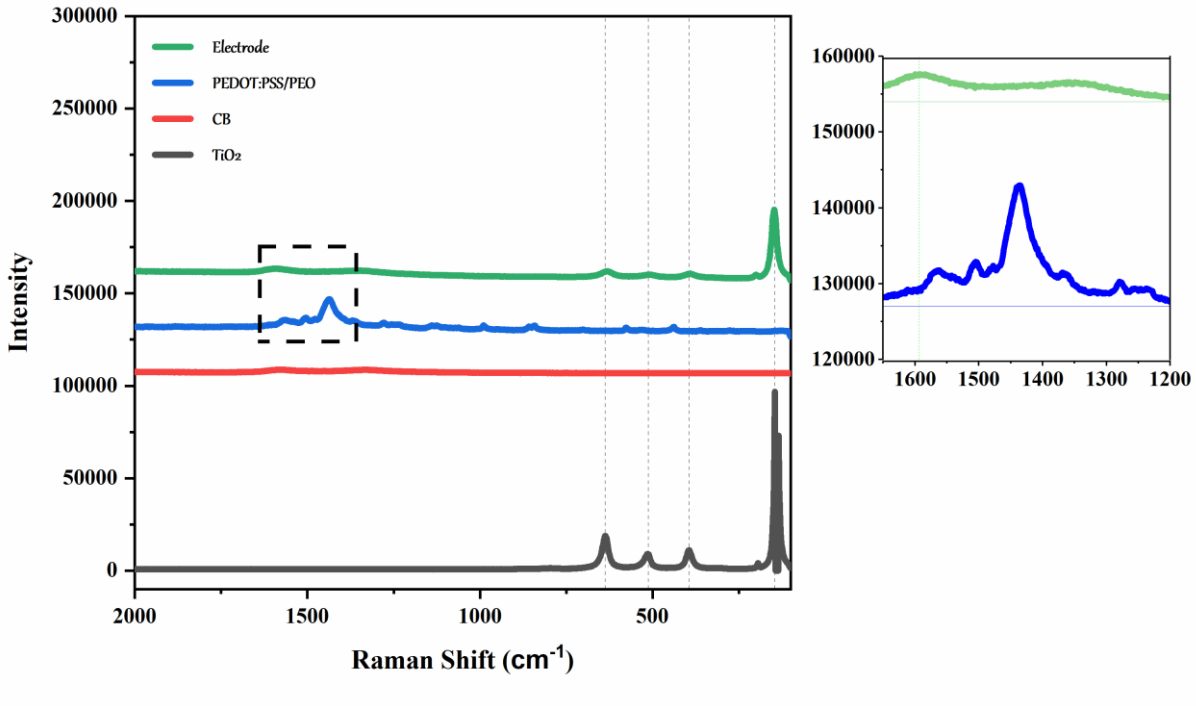

Figure 3-22. RAMAN spectra of the electrospun electrode besides the ones for TiO_2, CB, and PEDOT:PSS/PEO.

3.5 Electrochemical Analysis

After assembling the anode within the cell, it was remained untouched over night to build up a balance within the cell. Subsequently, the battery was gone under different analysis.

As shown in Figure 3-23, the voltage is scanned at 0.1 mVs^{-1} from 1 V to 3 V, and in return, it comes to 1 V, and the test was repeated for 10 cycles. Normal pair of peaks which were usually observed in the TiO_2 nanoparticles can be shown, cathodic and anodic current

peak at 1.67 and 2.19, respectively. Theses peaks are representative of the intercalation and deintercalation of Li^+ within the structure.

Generally, the fraction of anodic current peak over the cathodic one (i_{pa}/i_{pc}) indicates the state of equilibrium over the scan potential window. However, considering the inactivity of the CB in this potential window, presence of the of PEO/PEDOT:PSS leads to another shoulder (2.61 V) and accordingly perturbates the balance in the mentioned equilibrium.

Additionally, the separation of the potential peaks in the CV profile can show the overpotential needed for transformation of TiO_2 to Li_xTiO_2 [16, 18]. The separation of peak potential in the 1st cycle is 0.52 V which was reduced to 0.46 V after 10 cycles. This can be attributed to SEI formation and consequent improved conductivity.

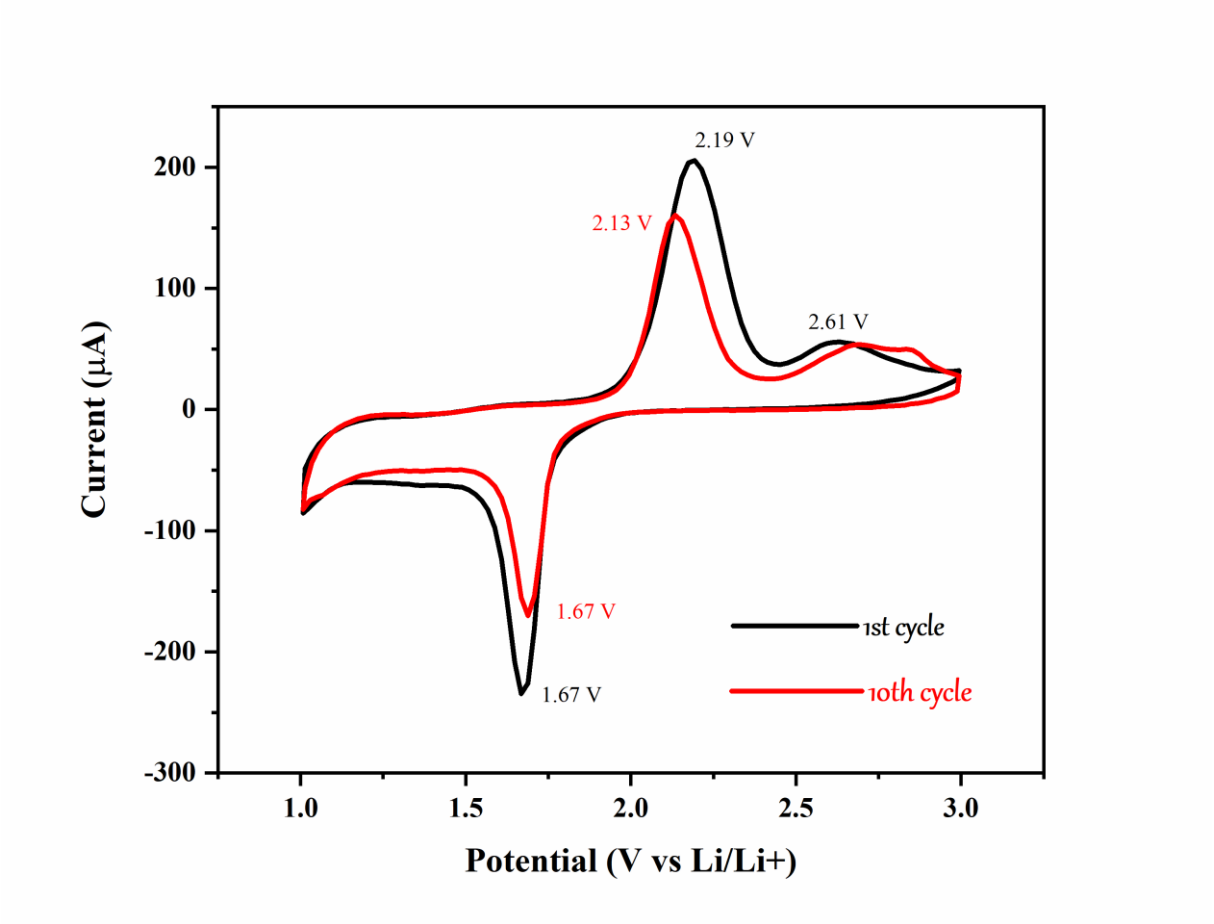

Figure 3-23. Cyclic voltammogram of the electrospun matrix in the 1-3 V voltage window with scan rate of 0.1 mV/s for 1st and 10th cycle.

The presence of this shoulder means that during charging more Li^+ can get out of the electrospun matrix (or cathode vs. Li foil), as a result, the area under the curve will increase and

lead to escalation of energy density. Formation of this shoulder for PEDOT:PSS was mentioned in the other studies as well [16, 46].

In order to measure behavior of the specific capacity of the anode, the galvanostatic charge discharge was tested at 0.1 C for the electrospun matrix (Figure 3-24).

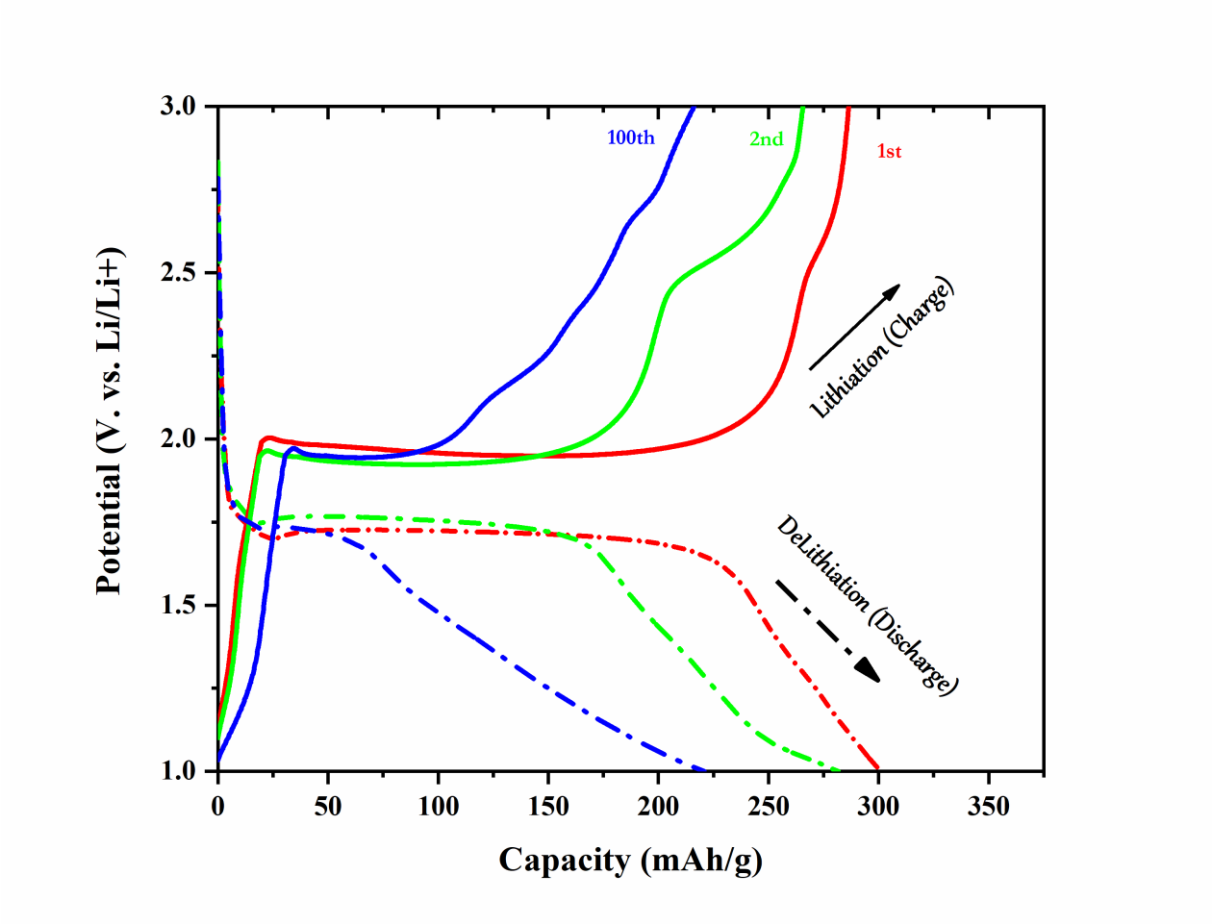

Figure 3-24. Voltage profile of lithiation and de-lithiation process for the electrospun electrode up to 100 cycles.

The discharge and charge cycling performance of electrospun electrode at 0.1 C was shown in Figure 3-24. The electrode illustrates large charge and discharge capacity with excellent cycling stability. At the 1st charge, the capacity reaches to 300 mAh^{-1}, which is less than the theoretical capacity for the TiO_2 (335 mAh g^{-1}). Furthermore, the discharge capacity experienced a rapid decline up to 6% (reaching to 263 mAh g^{-1}). However, afterwards, the capacity becomes relatively steady and coulombic efficiency didn't fall below 98% within 100 cycles (Figure 3-26).

The irreversible capacities may raise from different factors. One of the commonly mentioned factors is attribute to the intercalation of Li^+ to the irreversible sites and side

reactions [50]. The most important one can be the binding water remained from the ink preparation step. Since the Li^+ can irreversibly react with the water molecules and form Li_2O, which brought about the capacity loss [21]. However, after a few cycles the trace water was consumed, and capacity became stable.

The modest decline of the capacity after initial cycles can attribute to the formation of the SEI (passivation) layer. After completion of SEI formation, the built-up network can guarantee higher conductivity and long-lasting Li^+ diffusion in and out of the anode during lithiation and delaithiation, respectively [21]. The ac impedance spectroscopy may also prove the validity of this claim (Figure 3-25).

After fitting the data to an equivalent circuit using Z view software, the solution resistivity (R_s), the variation of the starting point of the semi-circles, was about constant through ten cycles (Table 3-3). Moreover, the diameter of semi-circle representing charge transfer impedance was increased from 40 to 42 Ω, which guarantees the decent connection between the electrolyte. Therefore, it was understood that the charge transfer impedance was kept constant and the consistency of the impedance shows the sustainable Li^+ cycling.

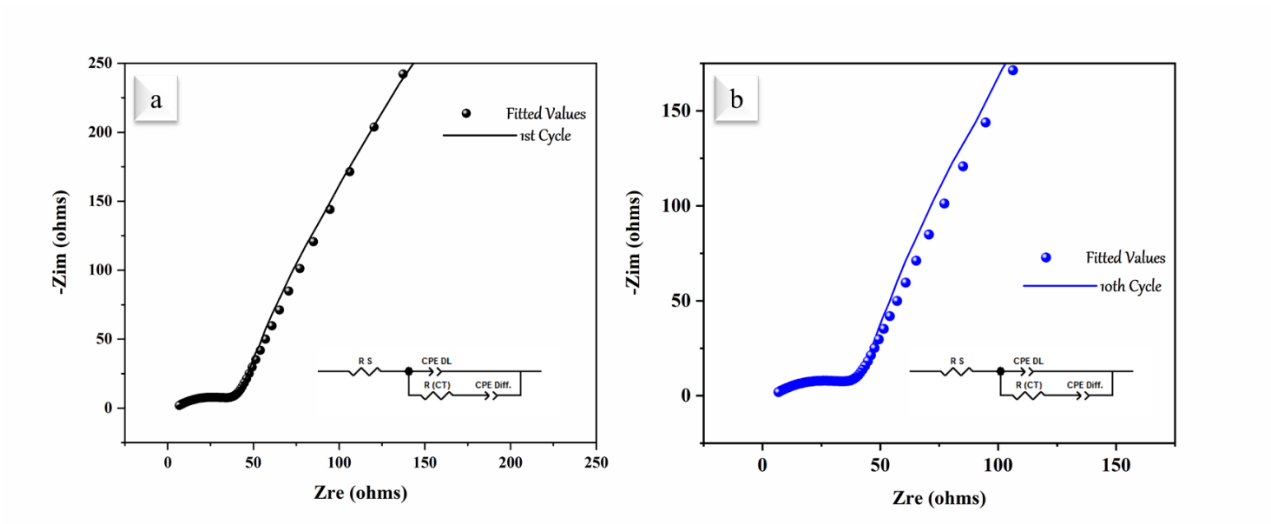

Figure 3-25. Nyquist plot of the assembled cell. Comparison of the impedance after first cycle with the one after 10 cycles.

Table 3-3. Fitted values for the EIS for the 1st and 10th cycles.

Element	Fitted for 1st cycle (ohms)	Error (%)	Fitted for 10th cycle (ohms)	Error (%)
R S	3.383	2.80	4.488	1.68
R (CT)	40.22	1.73	42.82	0.91

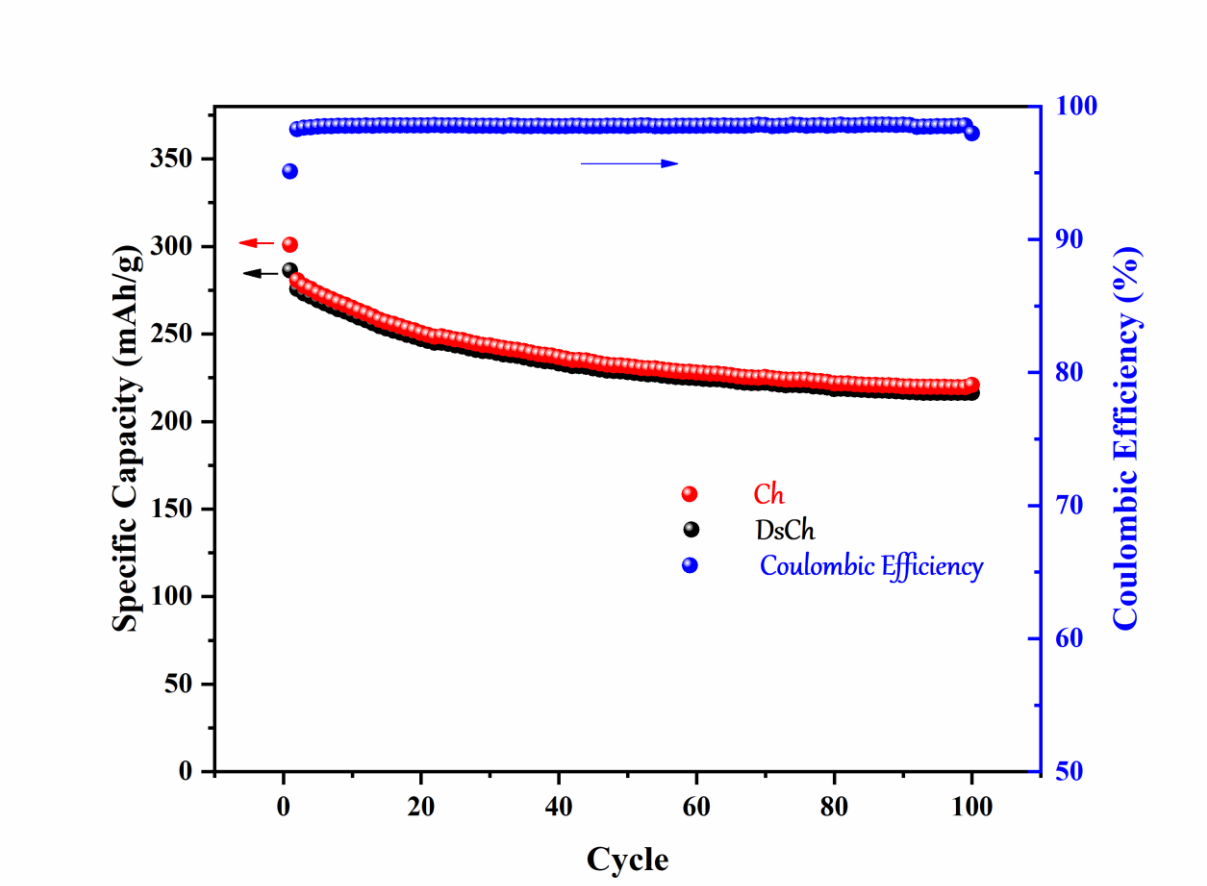

Figure 3-26. Specific capacity and coulombic efficiency of the electrospun electrode during charge/discharge cycling.

According to Figure 3-26, the capacity retention from 2nd cycle to the 100th cycle becomes 88.5% which shows a high reversibility. The average capacity fade for this range is 0.88% per cycle. After 80th cycle, capacity reached a steady state (around 230 mhA.g^{-1}) with 77% retention and 98% coulombic efficiency. The resulted reversibility is owning to the good electrical contant of the TiO_2 nanoparticles and the conductive agents (both PEDOT:PSS and CB) [21].

The charge cycling performance of electrospun electrode at different currents (0.1, 0.5, 1, and 2 C, separately) was shown in Figure 3-27. The electrode was able to deliver the 66% of the capacity at 0.5 C. Subsequently, the capacity was declined to 52 and 33% for 1C and 2C,

respectively. It is worthy to note that unless 0.1 C, there was always a decreasing trend for the capacities. After 20 cycles, the capacity could reach the 82% of the initial capacity.

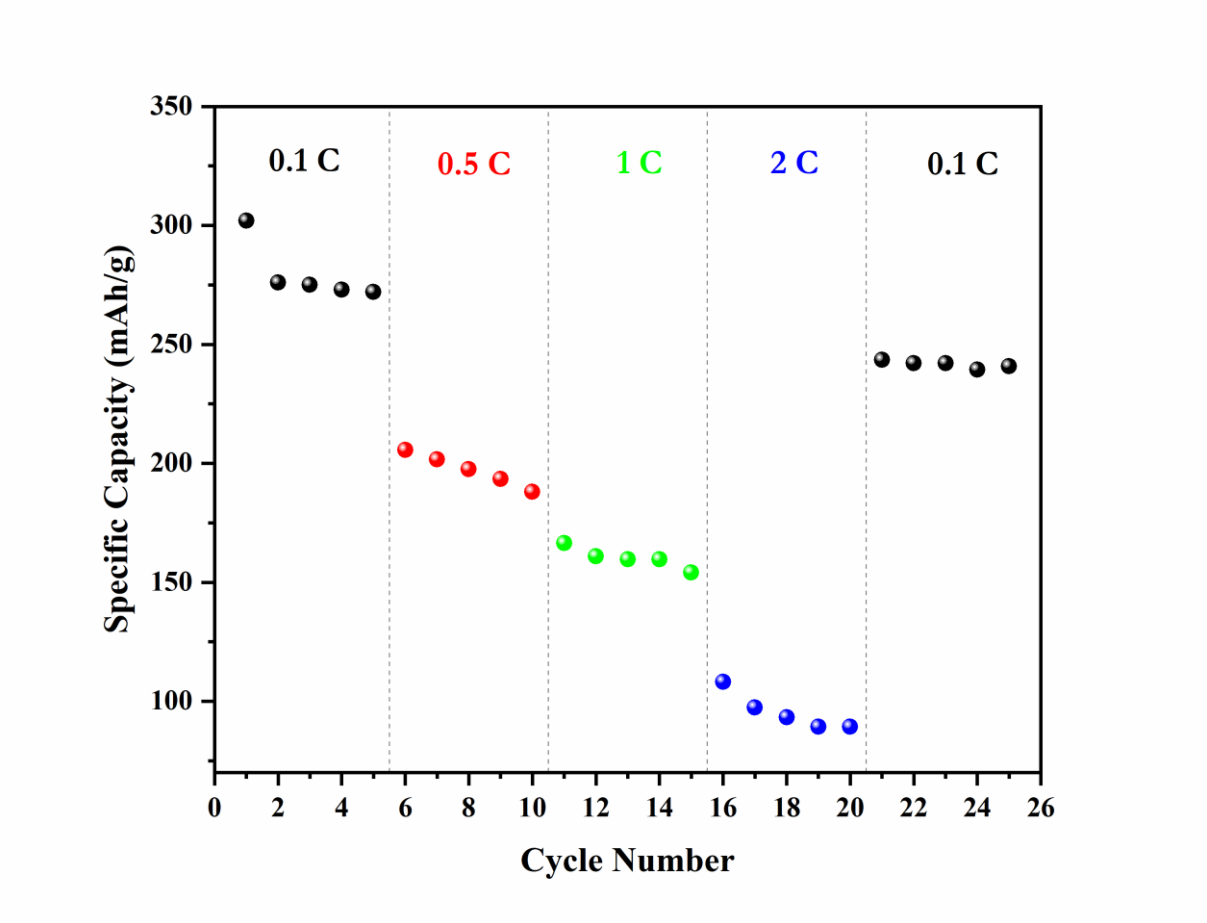

Figure 3-27. Rate performance test of the electrospun electrode (1C= 335 $mA.g^{-1}$).

In comparison with the research done in the similar current densities in Table 3-4, the produced anode shows a comparable capacity in the low current density region (33.5 $mA.g^{-1}$). However, by increasing the current density, the anodes with graphene additives show better performance. For instance, in 335 $mA.g^{-1}$, ordered mesoporous TiO_2/rGO composite reached 212 $mAh.g^{-1}$, even though, our electrospun anode won't exceed 170 $mAh.g^{-1}$. It worth noting that all the compared anode electrodes were prepared by casting of the active material with conductive agent on the Cu foil. Therefore, the Cu foil could be considered as a dead material in the anode. However, the fabricated anode lacks any substrates. Additionally, in all the other research the amount of binder (10-15 wt% of PVDF), as insulator, was also deemed as a dead material; even though, PEO/PEDOT:PSS fibers not only carried the active materials but also it contributed in both Li^+ storage as well as improved conductivity.

It is worth mentioning that the part of the higher specific capacities of the similar research is owning to the presence of graphene, 744 $mAh.g^{-1}$ [57]. Therefore, direct comparison of this study with the anodes containing graphene will fade the role of the PEDOT:PSS conductive agent. However, thanks to the promising behavior of PEDOT:PSS, addition of this agent may improve the performance of the already-high anodes to even better capacities as well.

Table 3-4. Comparison of the gravimetric specific capacity of TiO_2-based anodes with the present study.

Material	Voltage (V vs. Li^+/Li)	Current density ($mA.g^{-1}$)	Specific Capacity ($mAh.g^{-1}$)	Cycling Performance	Anode Type	Ref.
High performance N-doped mesoporous carbon decorated TiO_2 nanofibers	1-3	33	264	100	Casted on the Cu foil	[58]
$OMTiO_2$–rGO-NF	1-3	33.5	295	-	Casted on the Cu foil	[15]
		335	212	500		
		838	168	-		
Graphene/mesoporous TiO_2 sandwich-like nanosheets	1-3	20	237	100	Casted on the Cu foil	[53]
Porous TiO_2/C nanocomposite shells	1-3	335	171	230	Casted on the Cu foil	[54]
Ultrafine TiO_2 nanoparticles embedded in N-doped graphene networks	1-3	840	143	200	Casted on the Cu foil	[59]
TiO_2/GO nanocomposite	1-3	336	150	50	Casted on the Cu foil	[60]
This work	1-3	33.5	260	100	Self -Standing	-
		335	170	-		
		750	95	-		

To investigate the electrodes areal capacity, two different of electrode thicknesses were achieved. The anode loading for the 60 and 220 μm thicknesses were 1.42 and 3.41 $mg.cm^{-2}$, respectively. Thereby performing the charge/discharge cycling test, the areal capacities of electrode was calculated at various c-rates (Figure 3-28). The areal capacity was increased by increasing the thickness of the samples which can be attributed to the ability of porous structure to guarantee the good connection of electrolyte and active materials even at higher loading of the electrode.

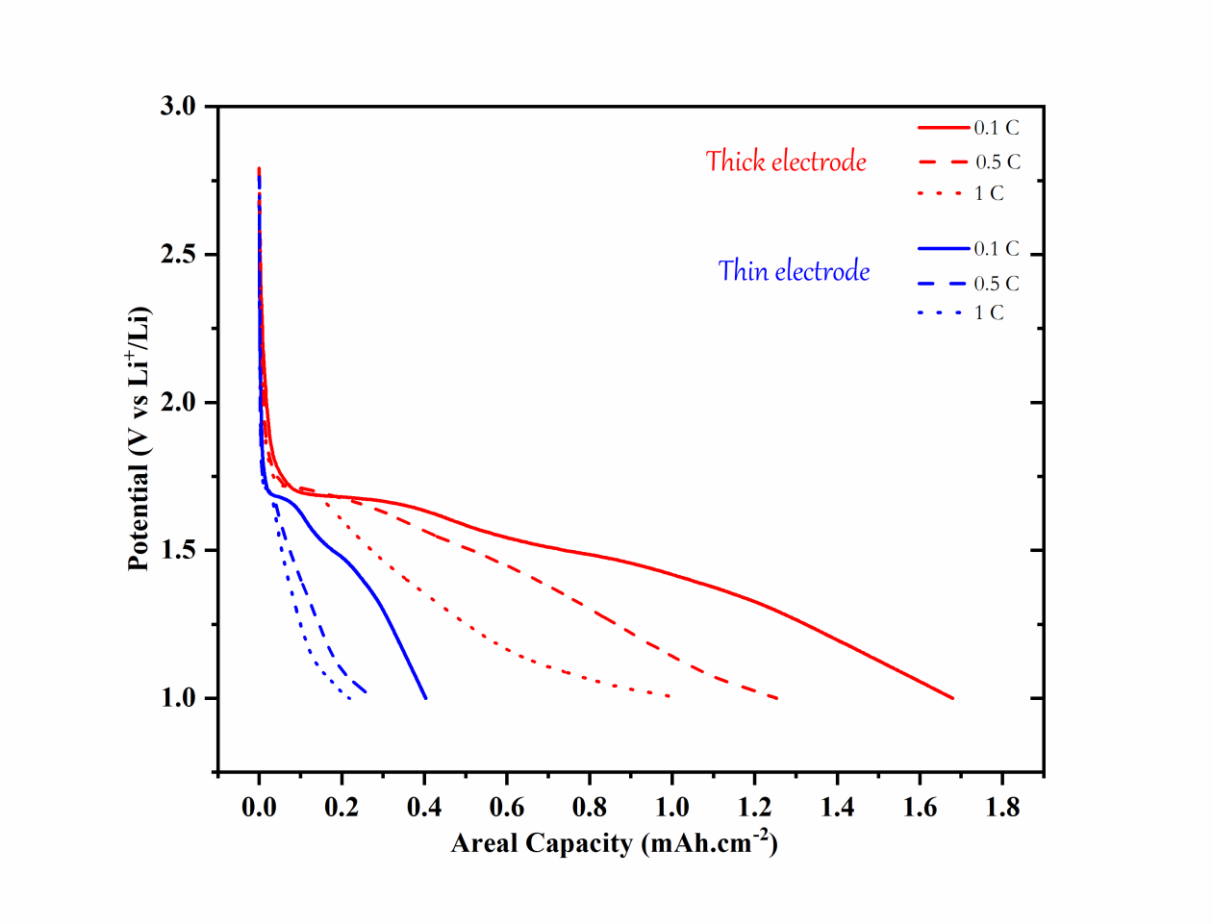

Figure 3-28. Comparison of areal capacity of the same electrode with two different thicknesses at 0.1, 0.5, and 1 C rates.

Comparison of the areal capacity of the electrode with other electrospun TiO_2-based materials won't be an accurate since the thickness and loading of the electrode cannot be similar. However, some improvements could be detected in anode electrode compared to the other studies. Therefore, the produced electrode not only could deliver same areal capacities compared with the similar electrospun electrodes (PAA/C/TiO_2) but also regarding gravimetric capacity, our electrospun mat could deliver much escalated capacities in comparison with other studies (Refs. [61] & [33]). As shown in Figure 3-30, the gravimetric capacity reached 300 $mAh.g^{-1}$ at 0.1 C; however, similar study using another conductive polymer (PAA) just reached a maximum capacity of 175 and 100 in two different studies (Refs. [61] & [33], respectively). Consequently, the more than doubled gravimetric capacity could be obtained.

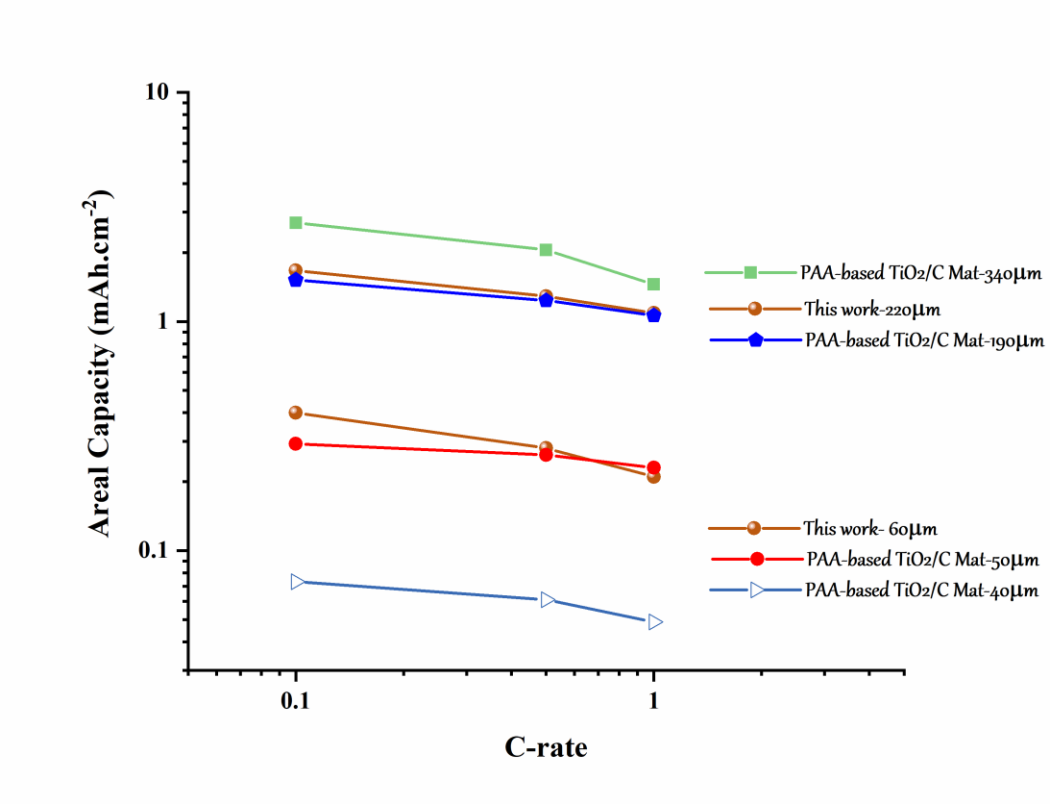

Figure 3-29. Comparison of areal capacity of electrospun TiO_2 with obtained data from Refs. [33, 61].

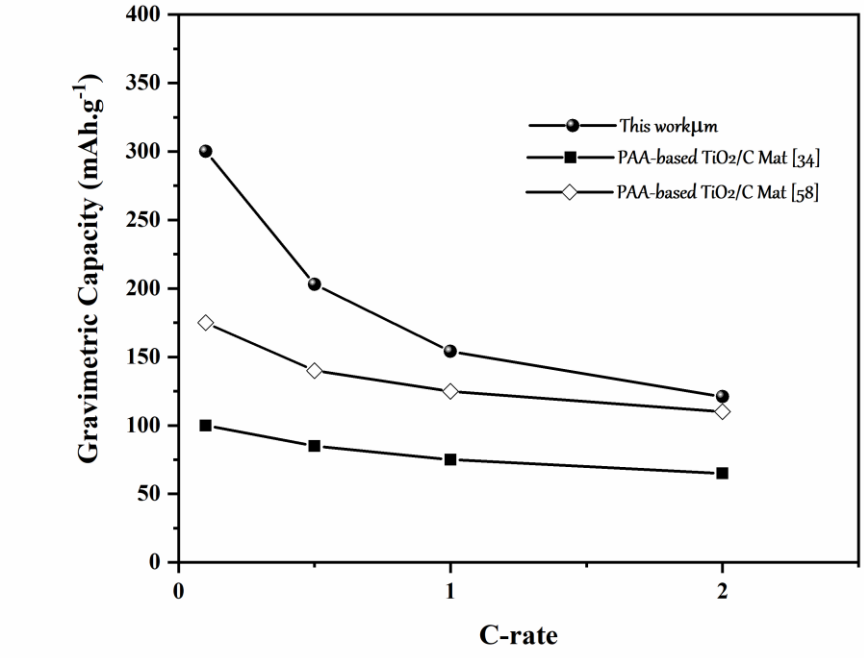

Figure 3-30. Comparison of the gravimetric capacity of the conductive polymer-based electrospun electrodes.

Due to the repeating of the folds in the commercial pouch cell batteries, the repeating units could be considered similar to Scheme 3-1. To clarify the improvements achieved by the fabrication of the anode in this research, the energy density of a hypothetical full cell comprised of the present anode and a high performance commercial cathode (NMC 333) was calculated and compared with one similar sample from Table 3-4.

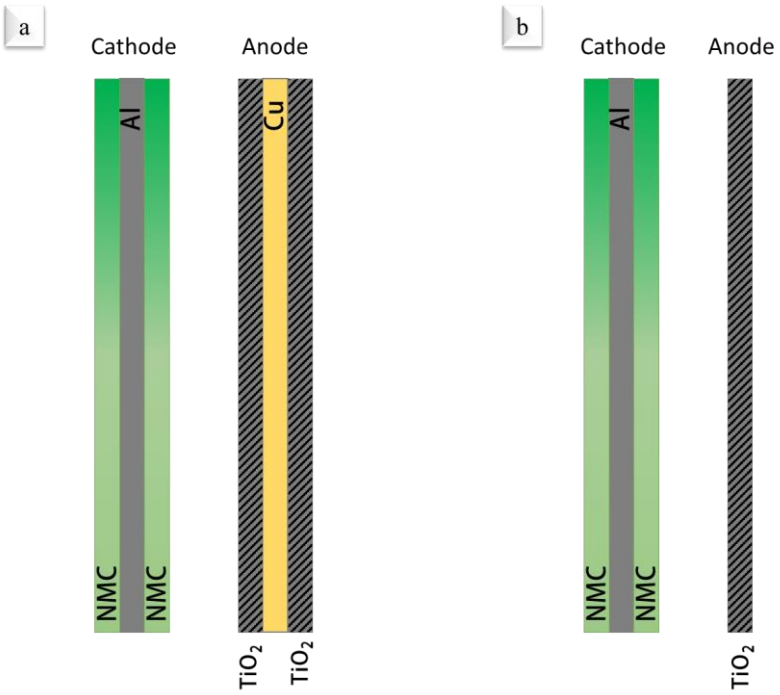

Scheme 3-1. Repetitive units in a pouch cell battery: a) Used anode was casted on both sides of the Cu foil, and b) anode is a free-standing electrospun matrix without Cu foil.

Similar to a real pouch cell battery, 0.286 m^2 of Cu and 0.263 m^2 Al foils were assumed for the anode and cathode substrates, respectively (since the electrospun mat is a free standing one, the Cu foil's weight was not added to the calculations). The Energy density of the hypothesized full cell can be obtained by the following equation:

$$Full\ Cell\ Energy\ Density\ = \frac{V_{nominal}(Cathode\ vs.\ Anode) \times Battery\ Capacity}{Battery\ Weight} \qquad (3\text{-}1)$$

Based on the data obtained from BatPaC software in Table 3-5, for a hypothesized pouch cell battery, the calculation of energy density can be performed. For sake of simplicity,

the common additional weight for all batteries including casing, electrolyte, connectors, and separator was deemed similar.

Table 3-5. Properties of the components in a real pouch cell battery for energy density calculations.

NMC 333 theoretical capacity	155 mAh/g
Active material participation in Cathode	96%
Ionization potential of Cathode	3.7 V
Anode theoretical Capacity	335 mAh/g
Ionization potential of Anode	1.67 V
Al Casing mass	10.1 g
Connectors mass	22.4 g
Electrolyte mass	0.042 g
Separator mass	3.348 g
Cu foil mass	25.62
Al foil mass	10.65

In order to understand the effect of Cu foil substrate in calculations, one ordinary case of the anode with Cu foil (which possesses a higher gravimetric capacity) was selected from Table 3-4 (N-doped mesoporous carbon decorated TiO_2 nanofibers) and compared with the resulted anode in this study. Considering 3 and 2.38 mg/mm^2 anode active material coating densities, the amount of the needed capacity for the full cell was measured as 3.21 and 1.87 Ah for battery with Cu foil and electrospun mat, respectively. By calculating the amount of needed cathode materials, 21.59 and 11.89 g of NMC333 were required to reach the sufficient capacity for the battery with Cu foil and electrospun mat, respectively. Thereby considering the other additional masses mentioned in Table 3-5 and the nominal voltage (2.03 V), the energy density of the Cu foil possessed battery and free standing electrospun mat were calculated as 63.15 and 70.9 Wh/kg, respectively.

Chapter 4. Conclusion

In this research, for the first time, PEDOT:PSS highly conductive polymer was used as a carrier polymer to produce a high-performance electrospun anode for the LIBs. Besides the conductivity of this polymer, the resulted electrochemical activity of the PEDOT:PSS-based electrode can also be improved. However, the major problem of the PEDOT:PSS was the low viscosity making the electrospinning of this polymer impossible. Therefore, a mixture of PEO/PEDOT:PSS was utilized to overcome the problem.

A systematic and laborious work was conducted to optimize the ink suitable for electrospining of the highly loaded electrode (TiO_2/CB/Polymer=70/20/10). Lots of parameters like PEO/PEDOT:PSS weight ratio (PR), PEO molecular weight, dispersants weight ratio (DMF/Water), polymer solid ratio, ink solid ratio, and prob sonication effect was optimized. In addition to ink preparation variables, operational parameters like relative humidity, applied voltage, feeding rate, needle to collector distance were also optimized.

Homogeneous loading of the fibers with average diameter of 2 μm in diameter was brought about when PR=5, DMF/Water=0.2, PEO molecular weight =1,000,000 g/mol. Other operational parameters for electrospinning were also thoroughly investigated using SEM Images. The best condition for electrospinning was achieved in 17-19 kV applied voltage, 0.8-1.2 mL/h flow rate, and 30% humidity with needle to collector distance of 12 cm.

Thereby performing electrochemical analysis, the gravimetric capacity of the electrospun mat (300 $mAh.g^{-1}$) was doubled in compared to the best anatase-based previously reported anodes (150 $mAh.g^{-1}$). At the same time, comparable areal capacities were achieved with the same material loadings (1.67 $mAh.cm^{-2}$) at 0.1 C. These improvements are owning to addition of the PEDOT:PSS resulting in: (i) improved conductivity deduced from the EIS test, and (ii) additional capacities to the CV curve because of the electroactivity of the carrier polymer.

Although the highest gravimetric capacities compared to the other studies with casting method was not achievable in this study, due to using a free-standing electrospun matrix in this study, higher energy densities can be obtained.

Chapter 5. References

1. Yuanli Ding, Zachary P. Cano, Aiping Yu, Jun Lu, Zhongwei Chen (2019) Automotive Li-Ion Batteries: Current Status and Future Perspectives. Electrochemical Energy Reviews 2(1):128
2. Hwang, Sooyeon and Stach, Eric A (2020) Using in situ and operando methods to characterize phase changes in charged lithium nickel cobalt aluminum oxide cathode materials. Journal of Physics D: Applied Physics 53(11): 113002.
3. Agus Purwanto, Cornelius Satria Yudha, U Ubaidillah, Hendri Widiyandari, Takashi Ogi, Hery Haerudin (2018) NCA cathode material: synthesis methods and performance enhancement efforts. Materials Research Express 5(12):122001
4. Lehao Liu, Meicheng Li, Lihua Chu, Bing Jiang, LinRuoxu, ZhuXiaopei, Guozhong Cao (2020) Layered ternary metal oxides_ Performance degradation mechanisms as cathodes, and design strategies for high-performance batteries. Progress in Materials Science 111:100655
5. Aravindan, V and Shubha, N and Ling, W Chui and Madhavi, S (2013) Constructing high energy density non-aqueous Li-ion capacitors using monoclinic TiO_2-B nanorods as insertion host. Journal of Materials Chemistry A 1(20):6145-6151
6. Jing, Mao-xiang and Li, Jing-quan and Han, Chong and Yao, Shan-shan and Zhang, Ji and Zhai, Hong-ai and Chen, Li-li and Shen, Xiang-qian and Xiao, Ke-song (2017) Electrospinning preparation of oxygen-deficient nano TiO_{2-x}/carbon fibre membrane as a self-standing high performance anode for Li-ion batteries. Royal Society Open Science 4(7):170323
7. Etacheri, Vinodkumar and Marom, Rotem and Elazari, Ran and Salitra, Gregory and Aurbach, Doron (2011) Challenges in the development of advanced Li-ion batteries: a review. Energy & Environmental Science 4(9):3243-3262
8. Gang Sun, Xucai Yin, Wu Yang, Ailing Song, Chenxiao Jia, Wang Yang, Qinghua Du, Zhipeng Ma, Guangjie Shao (2017) The effect of cation mixing controlled by thermal treatment duration on the electrochemical stability of lithium transition-metal oxides. Physical Chemistry Chemical Physics 19(44):29886-29894
9. Tianmei Chen, Yi Jin, Hanyu Lv, Antao Yang, Meiyi Liu, Bing Chen, Ying Xie, Qiang Chen (2020) Applications of Lithium-Ion Batteries in Grid-Scale Energy Storage Systems. Transactions of Tianjin University 26(3):208-217

10. Aurbach, Doron and Talyosef, Yosef and Markovsky, Boris and Markevich, Elena and Zinigrad, Ella and Asraf, Liraz and Gnanaraj, Joseph S and Kim, Hyeong-Jin (2004) Design of electrolyte solutions for Li and Li-ion batteries: a review. Electrochimica Acta 50(2-3):247-254
11. Pallavi Verma, Pascal Maire, Petr Novák (2010) A review of the features and analyses of the solid electrolyte interphase in Li-ion batteries. Electrochimica Acta 55(22):6332-6341
12. Debasish Mohanty, Jianlin Li, Daniel P. Abraham, Ashfia Huq, E. Andrew Payzant, David L. Wood, III, and Claus Daniel (2014) Unraveling the voltage-fade mechanism in high-energy-density lithium-ion batteries: origin of the tetrahedral cations for spinel conversion. Chemistry of Materials 26(21):6272-6280
13. Han, Yu and Huang, Guoyong and Xu, Shengming (2020) Structural Reorganization–Based Nanomaterials as Anodes for Lithium-Ion Batteries: Design, Preparation, and Performance. Small 16(15):1902841
14. Yang, Yang and Wang, Haiying and Zhou, Qiwen and Kong, Mengqi and Ye, Haitao and Yang, Gang (2013) Improved lithium storage properties of electrospun TiO_2 with tunable morphology: from porous anatase to necklace rutile. Nanoscale 5(21):10267-10274
15. Chattopadhyay, Shreyasi and Maiti, Sandipan and Das, Indranee and Mahanty, Sourindra and De, Goutam (2016) Electrospun TiO_2–rGO Composite Nanofibers with Ordered Mesopores by Molecular Level Assembly: A High Performance Anode Material for Lithium-Ion Batteries. Advanced Materials Interfaces 3(23):1600761
16. Yang, Zunxian and Du, Guodong and Meng, Qing and Guo, Zaiping and Yu, Xuebin and Chen, Zhixin and Guo, Tailiang and Zeng, Rong (2012) Synthesis of uniform TiO_2@ carbon composite nanofibers as anode for lithium ion batteries with enhanced electrochemical performance. Journal of Materials Chemistry 22(12):5848-5854
17. Guangfei He, Yibing Cai, Yong Zhao, Xiaoxu Wang, Chuilin Lai, Min Xi, Zhengtao Zhu, Hao Fong (2013) Electrospun anatase-phase TiO_2 nanofibers with different morphological structures and specific surface areas. Journal of colloid and interface science 398:103-111
18. He, Ben-Lin and Dong, Bin and Li, Hu-Lin (2007) Preparation and electrochemical properties of Ag-modified TiO_2 nanotube anode material for lithium-ion battery. Electrochemistry Communications 9(3):425-430
19. Min Su Jo, Gi Dae Park, Yun Chan Kang, Jung Sang Cho (2018) Design and synthesis of interconnected hierarchically porous anatase titanium dioxide nanofibers as high-rate and long-cycle-life anodes for lithium-ion batteries. Nanoscale 10(28):13539-13547

20. Oonhee Rhee, Gibaek Lee, and Jinsub Choi (2016) Highly ordered TiO_2 microcones with high rate performance for enhanced lithium-ion storage. ACS applied materials & interfaces 8(23):14558-14563
21. Wang, Yunfei and Wu, Muying and Zhang, WF (2008) Preparation and electrochemical characterization of TiO_2 nanowires as an electrode material for lithium-ion batteries. Electrochimica Acta 53(27):7863-7868
22. Armstrong, A Robert and Armstrong, Graham and Canales, Jesus and Garcia, Raquel and Bruce, Peter G (2005) Lithium-Ion Intercalation into TiO_2-B Nanowires. Advanced materials 17(7):862-865
23. Xu, Jinwei and Jia, Caihong and Cao, Bin and Zhang, WF (2007) Electrochemical properties of anatase TiO_2 nanotubes as an anode material for lithium-ion batteries. Electrochimica Acta 52(28):8044-8047
24. Qiao, Hui and Wang, Yawen and Xiao, Lifen and Zhang, Lizhi (2008) High lithium electroactivity of hierarchical porous rutile TiO_2 nanorod microspheres. Electrochemistry Communications 10(9):1280-1283
25. Kaikai Li, Baohua Li, Junxiong Wu, Feiyu Kang, Jang-Kyo Kim, and Tong-Yi Zhang (2017) Ultrafast-charging and long-life li-ion battery anodes of TiO_2-B and anatase dual-phase nanowires. ACS applied materials & interfaces 9(41):35917-35926
26. Zhu, Peining and Wu, Yongzhi and Reddy, MV and Nair, A Sreekumaran and Chowdari, BVR and Ramakrishna, S (2012) Long term cycling studies of electrospun TiO_2 nanostructures and their composites with MWCNTs for rechargeable Li-ion batteries. Rsc Advances 2(2):531-537
27. Thirugunanam, Lavanya and Kaveri, Satheesh and Etacheri, Vinodkumar and Ramaprabhu, Sundara and Dutta, Mrinal and Pol, Vilas G (2017) Electrospun nanoporous TiO_2 nanofibers wrapped with reduced graphene oxide for enhanced and rapid lithium-ion storage. Materials Characterization 331:64-71
28. Yameng Ren, Juan Zhang, Yanyan Liu, Hongbian Li, Huijuan Wei, Baojun Li, and Xiangyu Wang (2012) Synthesis and superior anode performances of TiO_2-carbon-rGO composites in lithium-ion batteries. ACS applied materials & interfaces 4(9):4776-4780
29. Hao Liu, Wei Li, Dengke Shen, Dongyuan Zhao, and Guoxiu Wang (2015) Graphitic carbon conformal coating of mesoporous TiO_2 hollow spheres for high-performance lithium ion battery anodes. Journal of the American Chemical Society 137(40):13161-13166
30. Karakaş H (2015) Electrospinning of nanofibers and their applications. Istanbul Technical University

31. Saeed Hamzeh, Mohsen Miraftab, and Ata Yoosefinejad (2014) Study of electrospun nanofibre formation process and their electrostatic analysis. Journal of Industrial Textiles 44(1):147-158
32. Quynh P. Pham Upma Sharma, Ph.D. Dr. Antonios G. Mikos, Ph.D. (2006) Electrospinning of Polymeric Nanofibers for Tissue Engineering Applications: A Review. Tissue engineering 12(5):1197-1211
33. Ethan C. Self, Ryszard Wycisk, Peter N. Pintauro (2015) Electrospun titania-based fibers for high areal capacity Li-ion battery anodes. Journal of power sources 282:187-193
34. Self, Ethan C and Naguib, Michael and Ruther, Rose E and McRen, Emily C and Wycisk, Ryszard and Liu, Gao and Nanda, Jagjit and Pintauro, Peter N (2017) High areal capacity Si/LiCoO2 batteries from electrospun composite fiber mats. ChemSusChem 10(8):1823-1831
35. ravindan, Vanchiappan and Sundaramurthy, Jayaraman and Kumar, Palaniswamy Suresh and Lee, Yun-Sung and Ramakrishna, Seeram and Madhavi, Srinivasan (2015) Electrospun nanofibers: A prospective electro-active material for constructing high performance Li-ion batteries. Chemical communications 51(12):2225-2234
36. Arico, Antonino Salvatore and Bruce, Peter and Scrosati, Bruno and Tarascon, Jean-Marie and Van Schalkwijk, Walter (2011) Nanostructured materials for advanced energy conversion and storage devices:148-159
37. Yu V Baskakova, O V Yarmolenko, O N Efimov (2012) Polymer gel electrolytes for lithium batteries. Russian Chemical Reviews 81(4):367
38. Yogesh Kumar, S.A. Hashmi, G.P. Pandey (2011) Lithium ion transport and ion–polymer interaction in PEO based polymer electrolyte plasticized with ionic liquid. Solid State Ionics 201(1):73-80
39. Bessaire, Bastien and Mathieu, Maillard and Salles, Vincent and Yeghoyan, Taguhi and Celle, Caroline and Simonato, Jean-Pierre and Brioude, Arnaud (2017) Synthesis of continuous conductive PEDOT: PSS nanofibers by electrospinning: A conformal coating for optoelectronics. ACS applied materials & interfaces 9(1):950-957
40. Galagan, Yulia and Rubingh, Jan-Eric JM and Andriessen, Ronn and Fan, Chia-Chen and Blom, Paul WM and Veenstra, Sjoerd C and Kroon, Jan M (2011) ITO-free flexible organic solar cells with printed current collecting grids. Solar Energy Materials and Solar Cells 95(5):1339-1343

41. Groenendaal, Lambertus and Jonas, Friedrich and Freitag, Dieter and Pielartzik, Harald and Reynolds, John R (2000) Poly (3, 4-ethylenedioxythiophene) and its derivatives: past, present, and future. Advanced materials 12(7):481-494
42. Gangopadhyay R, Das B, Molla MR (2014) How does PEDOT combine with PSS? Insights from structural studies. Rsc Advances 4(83):43912–43920
43. Bedford, Nicholas M and Winget, G Douglas and Punnamaraju, Srikoundinya and Steckl, Andrew J (2011) Immobilization of stable thylakoid vesicles in conductive nanofibers by electrospinning. Biomacromolecules 12(3):778-784
44. Zardalidis G, Mars J, Allgaier J, Mezger M, Richter D, Floudas G (2016) Influence of chain topology on polymer crystallization: Poly (ethylene oxide)(PEO) rings vs. linear chains. Soft Matter 12(39):8124–8134
45. Anitha, R and Menon, Sumithra S and Bhalerao, Gopalkrishna and Siddham, Pradeep and Baskar, K and Singh, Shubra (2020) Electrical properties of nitric acid and DMSO treated PEDOT: PSS/n-Si hybrid heterostructures for optoelectronic applications. Journal of Applied Polymer Science 137(32):48952
46. Trzciński, Konrad and Lisowska-Oleksiak, Anna (2015) Electrochemical characterization of a composite comprising PEDOT/PSS and N doped TiO_2 performed in aqueous and non-aqueous electrolytes. Synthetic Metals 209:399-404
47. Pradhan DK, Samantaray BK, Choudhary RNP, Thakur AK (2005) Effect of plasticizer on structure—property relationship in composite polymer electrolytes. Journal of power sources 139(1-2):384–393
48. Ungar, Tamas and Gubicza, Jen and Ribarik, Gabor and Pantea, Cristian and Zerda, T Waldek (2002) Microstructure of carbon blacks determined by X-ray diffraction profile analysis. Carbon 40(6):929-937
49. Hanaor, Dorian AH and Sorrell, Charles C (2011) Review of the anatase to rutile phase transformation. Journal of Materials science 46(4):855-874
50. Li, Junrong and Tang, Zilong and Zhang, Zhongtai (2005) Preparation and novel lithium intercalation properties of titanium oxide nanotubes. Electrochemical and Solid State Letters 8(6):A316
51. L.H. Sim, S.N. Gan, C.H. Chan, R. Yahya (2010) ATR-FTIR studies on ion interaction of lithium perchlorate in polyacrylate/poly(ethylene oxide) blends. Spectrochimica Acta Part A: Molecular and Biomolecular Spectroscopy 76(3-4):287-292

52. Prabhat Singh, Ashish Raman, Naveen Kumar (2020) Spectroscopic and Simulation Analysis of Facile PEDOT:PSS Layer Deposition-Silicon for Perovskite Solar Cell. Silicon 12(8):1769-1777
53. Wang, Zhiyu and Lou, Xiong Wen (2012) TiO_2 nanocages: fast synthesis, interior functionalization and improved lithium storage properties. Advanced materials 24(30):4124-4129
54. Wenshou Wang, Qina Sa, Jihua Chen, Yan Wang, Heejung Jung, and Yadong Yin (2013) Porous TiO_2/C nanocomposite shells as a high-performance anode material for lithium-ion batteries. ACS applied materials & interfaces 5(14):6478-6483
55. Arenas MC, Rodríguez-Núnez LF, Rangel D, Martínez-Álvarez O, Martínez-Alonso C, Castaño VM (2013) Simple one-step ultrasonic synthesis of anatase titania/polypyrrole nanocomposites. Ultrasonics sonochemistry 20(2):777–784
56. Hardcastle FD (2011) Raman spectroscopy of titania (TiO 2) nanotubular water-splitting catalysts. Journal of the Arkansas Academy of Science 65(1):43–48
57. Yao J, Shen X, Wang B, Liu H, Wang G (2009) In situ chemical synthesis of SnO_2–graphene nanocomposite as anode materials for lithium-ion batteries. Electrochemistry Communications 11(10):1849–1852
58. Myung-Hyun Ryu, Kyu-Nam Jung, Kyung-Hee Shin, Kyoo-Seung Han, and Sukeun Yoon (2013) High performance N-doped mesoporous carbon decorated TiO_2 nanofibers as anode materials for lithium-ion batteries. The Journal of Physical Chemistry C 117(16):8092-8098
59. Jiang, Xin and Yang, Xiaoling and Zhu, Yihua and Jiang, Hongliang and Yao, Yifan and Zhao, Peng and Li, Chunzhong (2014) 3D nitrogen-doped graphene foams embedded with ultrafine TiO_2 nanoparticles for high-performance lithium-ion batteries. Journal of Materials Chemistry A 2(29):11124-11133
60. Yongcai Qiu, Keyou Yan, Shihe Yang, Limin Jin, Hong Deng, and Weishan Li (2010) Synthesis of Size-Tunable Anatase TiO_2 Nanospindles and Their Assembly into Anatase@Titanium Oxynitride/Titanium Nitride−Graphene Nanocomposites for Rechargeable Lithium Ion Batteries with High Cycling Performance 4(11):6515-6526
61. Self, Ethan C and McRen, Emily C and Pintauro, Peter N (2016) High Performance Particle/Polymer Nanofiber Anodes for Liion Batteries using Electrospinning. ChemSusChem 9(2):208-215